Journal of Advanced Research in Applied Sciences and Engineering Technology

Journal homepage:
https://semarakilmu.com.my/journals/index.php/applied_sciences_eng_tech/index
ISSN: 2462-1943

Spreading and Splashing Dynamics of Bio-Oil Droplets upon Impaction on Inclined Metal Surfaces

Omer Khalid Shihab Ertobah[1], Khairil Faizi Mustafa[1,*], Khaled Ali Mohammad Al-attab[1]

[1] School of Mechanical Engineering, Tuanku Syed Sirajuddin Engineering Campus, 14300 Nibong Tebal, Penang, Malaysia

ARTICLE INFO

Article history:
Received 13 April 2026
Received in revised form 31 May 2026
Accepted 2 June 2026
Available online 10 June 2026

Keywords:

Droplet impact; inclined surface; bio-oil; Weber number; surface roughness

ABSTRACT

Droplet impact on inclined metallic surfaces is critical in heat transfer, coating, and bio-oil delivery systems; however, existing studies have largely focused on low-viscosity fluids and horizontal surfaces, with limited understanding of high-viscosity bio-oils under inclined and rough surface conditions. This study systematically examines the impact dynamics of droplets composed of olive, peanut, sunflower, and a 50% waste–50% olive oil blend on aluminium, copper, mild steel, and stainless steel at room temperature. Droplets with diameters of 2.6–3.2 mm were released at velocities of 3.96 m/s to 4.54 m/s, corresponding to Weber numbers of 923–1214, onto substrates inclined at 5° to 60° with surface roughness Ra ≈ 0.1 to 2.2 µm. High-speed imaging was employed to capture droplet deformation, spreading, and instability during impact. The results display that increasing inclination disrupts spreading symmetry and promotes downslope elongation, while higher inertia enhances deformation and may induce localized splashing. Surface roughness exhibits a regime-dependent effect, where rougher surfaces facilitate contact-line pinning and suppress spreading, whereas smoother surfaces promote lamella mobility and splashing, particularly for low-viscosity liquids. Moreover, fluid viscosity plays a critical stabilizing role, with bio-oils resisting jetting and fragmentation compared to water. These findings demonstrate the coupled effects of inertia, inclination, surface roughness, and fluid properties on droplet impact dynamics, providing a unified physical understanding and practical guidance for optimizing spray cooling, coating, and fuel deposition processes on inclined metallic surfaces.

1. Introduction

Droplet impact on solid surfaces governs key momentum, heat, and mass transfer processes in fuel spray cooling, quenching, combustion, and energy-system heat transfer applications. Upon impact, droplets may spread, splash, rebound, or fragment depending on inertia, viscosity, surface tension, gravity, surface roughness, and thermal conditions. Droplet impact regimes are central to applications such as spray and mist cooling [1,2], quenching [3], nuclear reactor [4,5], porous surface

* *Corresponding author.*
E-mail address: mekhairil@usm.my

https://doi.org/10.37934/araset.60.5.170194

interactions [6,7], steam turbines [8], and internal combustion engines [9,10]. In practical energy systems, droplets frequently interact with inclined metallic surfaces, where gravity-induced asymmetry fundamentally alters lamella evolution and contact-line motion compared to horizontal surfaces. Most existing droplet impact models have been developed for horizontal surfaces and idealized fluids, limiting their relevance to realistic energy-system geometries. In addition, most foundational studies underlying these applications are based on low-viscosity, single-component liquids, limiting their applicability to emerging renewable fuels such as bio-oils. This limitation hinders the extension of classical droplet impact theory to bio-oil-relevant systems. Surface inclination introduces gravity-driven asymmetry that modifies spreading and splash thresholds in a manner that cannot be captured by horizontal-surface scaling laws.

Extensive experimental and theoretical studies have established droplet impact regimes for low-viscosity Newtonian liquids under controlled hydrodynamic and thermal conditions. The effects of surface roughness and viscosity on spreading and bouncing have been widely reported [11,12], while early-stage impact dynamics have been correlated using Weber [13] and Reynolds numbers [14,15]. In addition, the influence of surface roughness on droplet's repellency was also investigated at different Weber values [16]. However, the precise role of surface topography remains unresolved, particularly for highly viscous liquids such as bio-oils. Thermal phenomena such as contact vaporization and Leidenfrost transitions further influence impact outcomes at elevated temperatures [15-17]. Regime maps and correlations are predominantly derived from single-component, low-viscosity liquids such as water and light hydrocarbons. Therefore, these regimes are insufficient to describe bio-oil droplet impaction. Classical impact scaling laws may fail for viscous, multicomponent fuel droplets due to enhanced viscous dissipation and altered wetting behavior.

Bio-oils and biodiesel fuels exhibit elevated viscosity, multicomponent composition, and strong coupling between thermophysical properties, which significantly influence droplet spreading, recoil, and evaporation. Unlike conventional fuels, bio-oil droplets may either evaporate rapidly at high temperatures or remain pinned in prolonged sessile states, suppressing recoil and splashing [18]. Isothermal studies of bio-oil droplet impact have reported sluggish spreading and saturation of maximum spreading diameter [19]. At high temperature, the impact patterns of droplets are mildly influenced by an increased in the surface temperature and a change in the inclination angle but the findings are limited to a water droplet [20]. Bio-oil droplet impact behavior has largely been studied under isothermal or weakly thermal conditions, which do not fully represent operating environments in energy and combustion systems. Thermal gradients will amplify differences between bio-oil and conventional fuel impact dynamics by strengthening the coupling between evaporation and hydrodynamic deformation.

Multicomponent evaporation models have demonstrated that fuel composition strongly affects droplet lifetime and evaporation rate, often deviating from classical d^2-law behavior [21-23]. While these models provide valuable insight into isolated droplet evaporation, they do not account for impact-induced spreading, recoil, and breakup on solid surfaces. Surface orientation and externally imposed flow fields further complicate droplet impact dynamics. Crossflow studies have shown pronounced deformation and directional breakup for both conventional and bio-derived fuel droplets, highlighting the importance of liquid-specific instability mechanisms [24]. In parallel, inclined-surface studies using water and low-viscosity fluids have revealed asymmetric spreading and altered splash initiation [25-28]. However, systematic investigations of bio-oil droplets impacting inclined metallic substrates with realistic roughness levels remain scarce [29,30]. Existing inclined-surface studies are dominated by model fluids and do not capture the rheological complexity of bio-based fuels. Bio-oil droplets are expected to exhibit stronger inclination-dependent regime shifts than low-viscosity liquids due to enhanced viscous dissipation and contact-line pinning.

Previous studies have established important droplet impact regimes for low-viscosity liquids on horizontal or mildly inclined surfaces, but these findings do not fully represent the behavior of bio-oil droplets on realistic metallic substrates. In particular, the combined effects of surface inclination, roughness, and bio-oil viscosity on spreading asymmetry, pinning, and splash initiation remain insufficiently understood. Existing regime maps are largely based on single-component model liquids and therefore provide limited guidance for multicomponent renewable fuels. Consequently, a systematic investigation of bio-oil droplet impact on inclined metallic surfaces is needed to clarify the governing physical mechanisms and support predictive design for energy and fuel applications.

This study systematically examines the impact behavior of bio-oil droplets on inclined metallic surfaces with varying roughness in order to clarify the coupled roles of liquid viscosity, surface inclination, and topography in controlling spreading and splash dynamics. High-speed imaging is used to resolve the impact process and to identify how these variables influence asymmetry, pinning, elongation, and breakup. The resulting analysis provides a basis for improved physical interpretation and predictive design of droplet-based processes involving renewable fuels on inclined engineering surfaces.

2. Methodology

A schematic diagram of the experimental setup is shown in Figure 1. A syringe pump-based droplet generation device (New Era Pump Systems, Inc. Model NE-1000, USA) was utilized to produce a single droplet of regulated size and velocity. The syringe output, without a needle, produced the droplet that fell under its own weight and struck the test surface from a specified release height H. The droplet velocity and Weber number, We were changed by adjusting the height at four vertical positions of 20cm, 50cm, 80cm, and 105cm. The vertical position was adjusted using a precision steel rack. A detached droplet, which fell under its own weight, had an equivalent diameter, D which was determined from Eq. (1)[31].

$$D = \left(D_x^2 \times D_y\right)^{1/3} \quad (1)$$

D_x and D_y denote the horizontal and vertical diameters of the droplet, respectively. The difference in the horizontal and vertical diameters was at most 0.09 mm. Four metal surfaces were used: aluminum, copper, mild steel, and stainless steel. These metal surfaces were alternately placed on a movable platform that enabled accurate angle inclination of 5°, 10°, 30°, 45°, and 60°. Surface roughness, Ra was determined using a surface roughness tester (Mitutoyo SV-3100S4, Japan). The measured Ra values for each surface are summarized in Table 1. High-resolution 3D surface topography was captured using a profilometer (Alicona Infinitefocus G4, Austria) and the surface topographies are shown in Figure 2.

The surface topography provides a detailed 3D mapping of all surfaces, characterizing its roughness and waviness. A 1500 W light emitting diode (LED) light source, along with a diffuser for uniform backlighting, illuminated the scene, while a high-speed camera (OLYMPUS i-speed Model 800-505-ATEC 2832, Olympus Corporation, Japan) running at 2000 fps, 800 x 800-pixel square images, captured the droplet impact, spreading, sliding, and splashing events.

The camera was oriented perpendicular to the droplet motion plane and linked to a computer system for data collection and image processing the camera was perfectly oriented to the horizontal axis (0° forward angle) to minimize the glaring effect and eliminate the unwanted distortion of the captured images. The target area on the metal surface was purposedly focused to be considerably small (approximately 8 mm × 8 mm) to simplify the impact process and made easier understanding

of the hydrodynamics particularities, which could be hindered by the effects of the liquid/solid viscous friction. When the droplet entered the focused area or the field of view, the image based auto triggering sensor automatically detected the darkened pixel and the recording was initiated. To measure the impact droplet velocity, two successive images were analyzed. These images provided the vertical distance between the falling droplet and the impact surface. The image processing software was later applied to threshold the droplet and remove odd backgroud shadows. Using the time interval between these successive images and the translational distance of the droplet, the impact droplet velocity, V_i was calculated using Eq. (2).

$$V_i = \frac{\Delta l}{\Delta t} \tag{2}$$

Δl is the vertical distance traveled by the droplet and Δt is the time lapse between two successive images. The theoretical impact droplet velocity, V_{th} was also calculated using Eq. (3)

$$V_{th} = \sqrt{2g(h - D_o)} \tag{3}$$

g and h represent the gravitational acceleration and the free-falling height of the droplet, respectively. From Eqs. (2) and (3), the mean percentage error, ε_{mean} was determined using Eq. (4) to estimate the error between the theoretical and experimental droplet impact velocity.

$$\varepsilon_{mean} = \frac{1}{N}\sum_{i=1}^{N}\left(\left|\frac{V_i - V_{th}}{V_{th}}\right| \times 100\right)_i (\%) \tag{4}$$

In this work, we produced the droplet velocities in the range of 3 to 5 m/s to observe different regimes and stages of impact dynamics. Weber number, We, which is defined as the ratio between the inertial force and surface tension force was determined from Eq. (5).

$$We = \frac{\rho V_i^2 D_o}{\sigma} \tag{5}$$

ρ is the density and σ is the surface tension of the droplet. The We values obtained in the experiment were found to be between 923 and 1214. When the impact surface is a plane solid substrate, as in the present study, the impact dynamics and behavior are primarily controlled by the droplet inertia, viscosity, surface tension, physical characteristics, and substrate parameters. All experiments were performed at atmospheric pressure (1 atm), room temperature (28 ºC), and relative humidity of approximately 80%.

Four bio-oils: olive oil, peanut oil, sunflower oil, and a 50% waste–50% olive oil (WCOO) were chosen as tested liquids. In addition, distilled water was also used as benchmark liquid to provide comparative assessment. Olive oil, peanut oil, and sunflower oil were acquired from a local supplier and the waste cooking oil was collected after domestic use.

The WCOO was prepared by measuring the mass of WCOO (the accuracy of a digital weighing scale was within $\pm$0.1g) and the mixture was subsequently placed in a domestically available bath chamber. It was continually exposed to an ultrasonic agitation. The WCOO was allowed to stabilize for 48h in a transparent tank and the mixture was observed for its miscibility during this period.

The physical properties, such as density, viscosity, and surface tension, were measured at room temperature using a precision balance, a rotational viscometer, and a Du Noüy ring tensiometer, respectively. The measured values are shown in Table 2. The data were utilized to calculate dimensionless parameters, including the We, Re, and Oh numbers, which dictate the observed

impact dynamics. A dimensionless time scale $\tau = tU_o/D_o$ was also determined for the purpose of standardizing temporal data, facilitating comparison across fluids and surfaces.

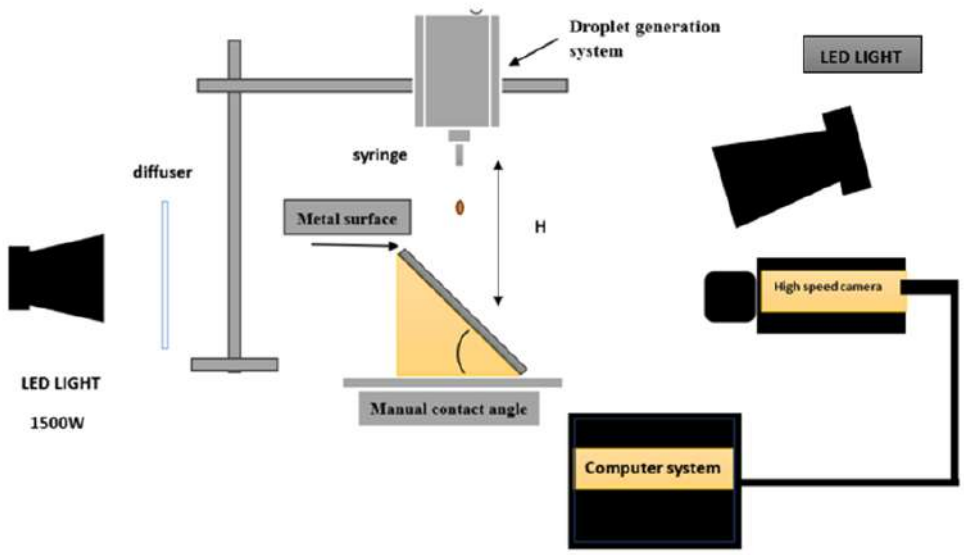

Fig. 1. Experimental setup for droplet impact on inclined metallic surfaces, showing the droplet generator, inclined substrate, LED illumination, and high-speed imaging system

Table 1
Surface materials, surface roughness, and dimensions

Surface Material	Ra with sandpaper (µm)	Ra without Sandpaper (µm)	Dimensions L × W × H (mm)
Aluminum (Al)	0.5448	0.7364	300 × 300 × 5
Stainless Steel (SS)	2.2229	1.9051	300 × 300 × 5
Mild Steel (Ms)	1.1728	0.9597	300 × 300 × 5
Copper (Cu)	0.3488	0.3729	300 × 300 × 5

Table 2
Physical properties of bio-oils at 25 °C

Bio-oil	density (kg/m^3)	surface tension N/m	viscosity (cp)
Olive	892.8	0.0383	43.79
Sunflower	858.3	0.0360	34.32
Peanut	827.4	0.0353	39.17
WCOO	883.3	0.0356	40.4
Distilled water	990.9	0.0720	1

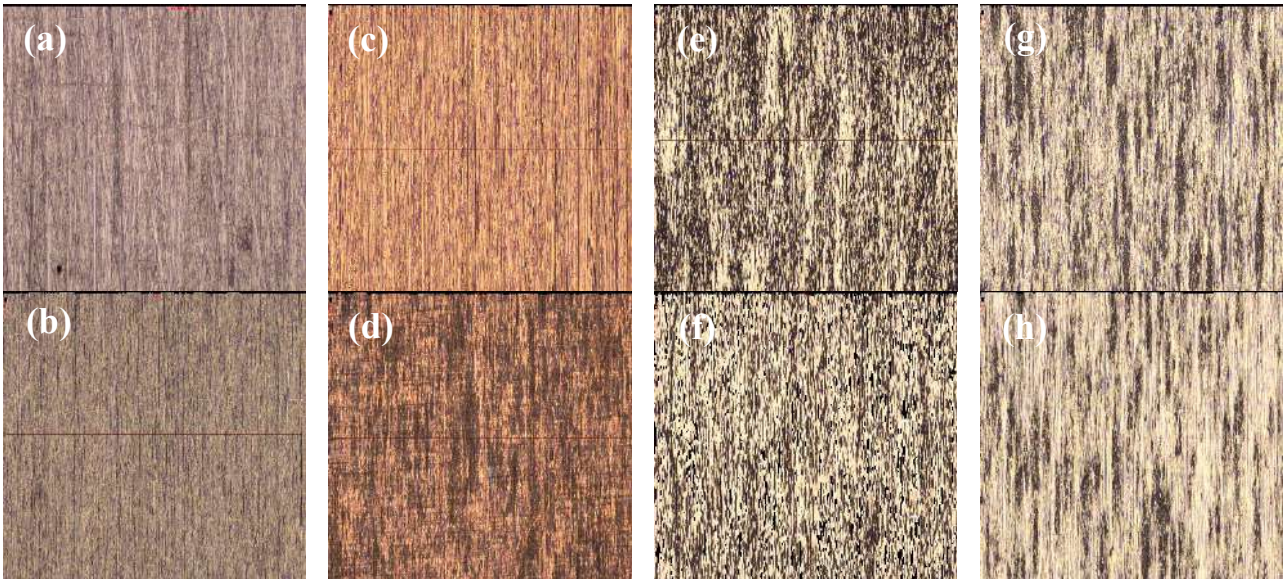

Fig. 2. Topography surface images (a) aluminum, Ra = 0.5448 µm (b) aluminum, Ra = 0.7364 µm (c) copper, Ra = 0.3488 µm (d) copper, Ra = 0.3729 µm (e) mild steel, Ra = 1.1728 µm (f) mild steel, Ra = 0.9597 µm (g) stainless steel, Ra = 2.2229 µm (h) stainless steel, Ra = 1.9051 µm

3. Results

This section describes the observed kinetics of bio-oil and water droplet interactions on inclined metal surfaces at room temperature. The study focuses on four aspects (i) spreading and sliding dynamics at low (5° and 10°), moderate (30°) and high (45° and 60°) inclination angles, (ii) the effect of We number on asymmetric spreading, (iii) the effect of surface roughness and inclination on lamella pinning, and (iv) comparative analysis of water and bio-oils that emphasizes the importance of viscosity and surface tension. The experimental results reveal a clear hierarchy of controlling parameters governing droplet impact dynamics. The Weber number acts as the primary parameter, as it represents the balance between inertial and surface tension forces and determines the onset of spreading and splashing. Surface inclination plays a secondary role by introducing gravitational asymmetry, which governs downslope elongation and directional spreading. Surface roughness has a limited influence at moderate Weber numbers but becomes increasingly important at higher inertia, where it enhances contact-line pinning and suppresses lamella instability. Fluid viscosity provides an additional stabilizing effect by dissipating kinetic energy, thereby delaying or preventing splash formation.

3.1 Spreading and Sliding at Low and High Inclination Angles

The spreading and sliding dynamics of bio-oil and water droplets were investigated at an impact velocity of 3.96 m/s (We ≈ 923) over inclination angles of 5°, 10°, 30°, 45°, and 60°. The definitions of droplet size D, horizontal droplet elongation X, and vertical droplet elongation Y are illustrated in Figure 3. At small inclination angles of 5° and 10°, all droplets exhibited nearly symmetric spreading with only minor downslope elongation. High-speed image sequences in Figs. 4 and 5 confirm that bio-oils stabilized quickly and remained intact, whereas water rims thinned and developed early instabilities. Due to the large number of images acquired, only representative cases are presented. Surface roughness had only a marginal influence on spreading at low inclination angles because the tangential momentum component of the droplet remained relatively small. Under these conditions, droplet behaviour was governed primarily by the balance between inertial and surface tension

forces, while surface irregularities played only a secondary role. At a moderate inclination angle of 30°, gravitational effects became more pronounced, leading to asymmetric spreading and enhanced downslope elongation. Bio-oils reached maximum spreading ratios of X/D ≈ 3.0–3.9 and Y/D ≈ 0.8–1.7, whereas water spread more extensively, with X/D = 6.5–7.9 and Y/D = 1.6–3.0. Bio-oils elongated slightly downslope (Y/D ≈ 1.3–1.6) while maintaining cohesive lamellae, whereas water exhibited significantly greater spreading and rivulet-like flow, as shown in Figure 6. These observations indicate that inclination increasingly modifies droplet behaviour by introducing gravitational asymmetry, which enhances downslope momentum and promotes directional spreading. At high inclination angles of 45° and 60°, asymmetry became dominant. Bio-oils compacted in the streamwise direction (X/D reduced to 2.5–3.0) but elongated significantly downslope (Y/D = 4.0–5.0), remaining largely splash-free due to viscous damping. In contrast, water footprints became unstable: at 45°, X/D peaked at 7.8–8.3 with Y/D ≈ 7.2–7.4, while at 60°, water collapsed strongly in the downslope direction with X/D ≈ 4.5 but Y/D > 11, accompanied by rim breakup and secondary droplet formation (Figs. 7 and 8). This behaviour indicates that gravitationally induced tangential momentum increasingly interacts with inertial forces at steep inclinations, amplifying spreading asymmetry and destabilizing low-viscosity fluids. In contrast, the higher viscosity of bio-oils dissipates kinetic energy and stabilizes the lamella, thereby suppressing fragmentation and splash initiation. As shown in Figure 9, water extended even further downslope (Y/D > 12) and splashed violently at higher impact velocity, whereas oils elongated moderately (Y/D ≈ 5–6) but remained cohesive. These results demonstrate that increasing inertia intensifies asymmetry and splash tendencies in low-viscosity fluids, while bio-oils maintain stable spreading due to enhanced viscous dissipation and contact-line stability. Overall, the results identify two distinct spreading regimes: (i) shallow inclinations, where spreading remains nearly symmetric and bio-oils resist sliding, and (ii) steep inclinations, where gravitational asymmetry enhances downslope elongation and destabilizes water but not bio-oils. Collectively, these results confirm that droplet behaviour is governed by the coupled interaction of inertia, gravitational effects, viscosity, and surface interaction mechanisms rather than by inclination angle alone.

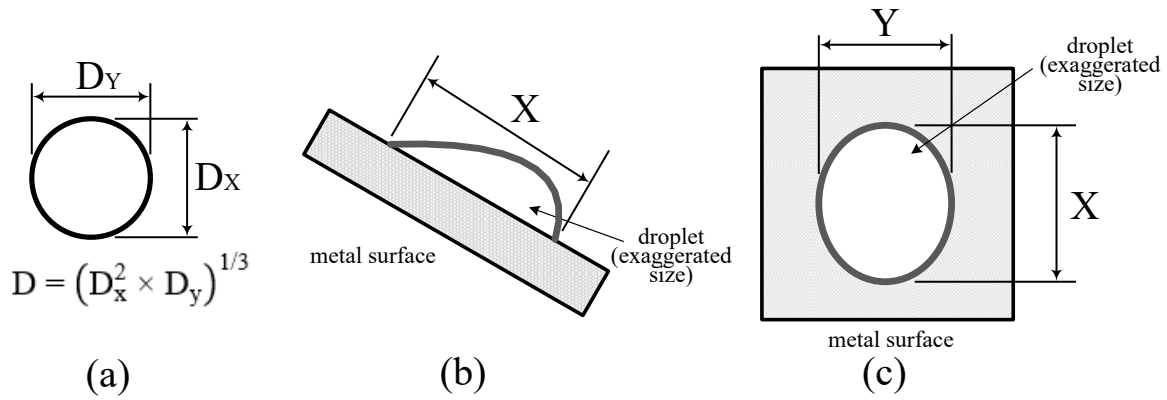

Fig. 3. (a) Definition of droplet size D (b) horizontal droplet elongation X (c) vertical droplet elongation Y

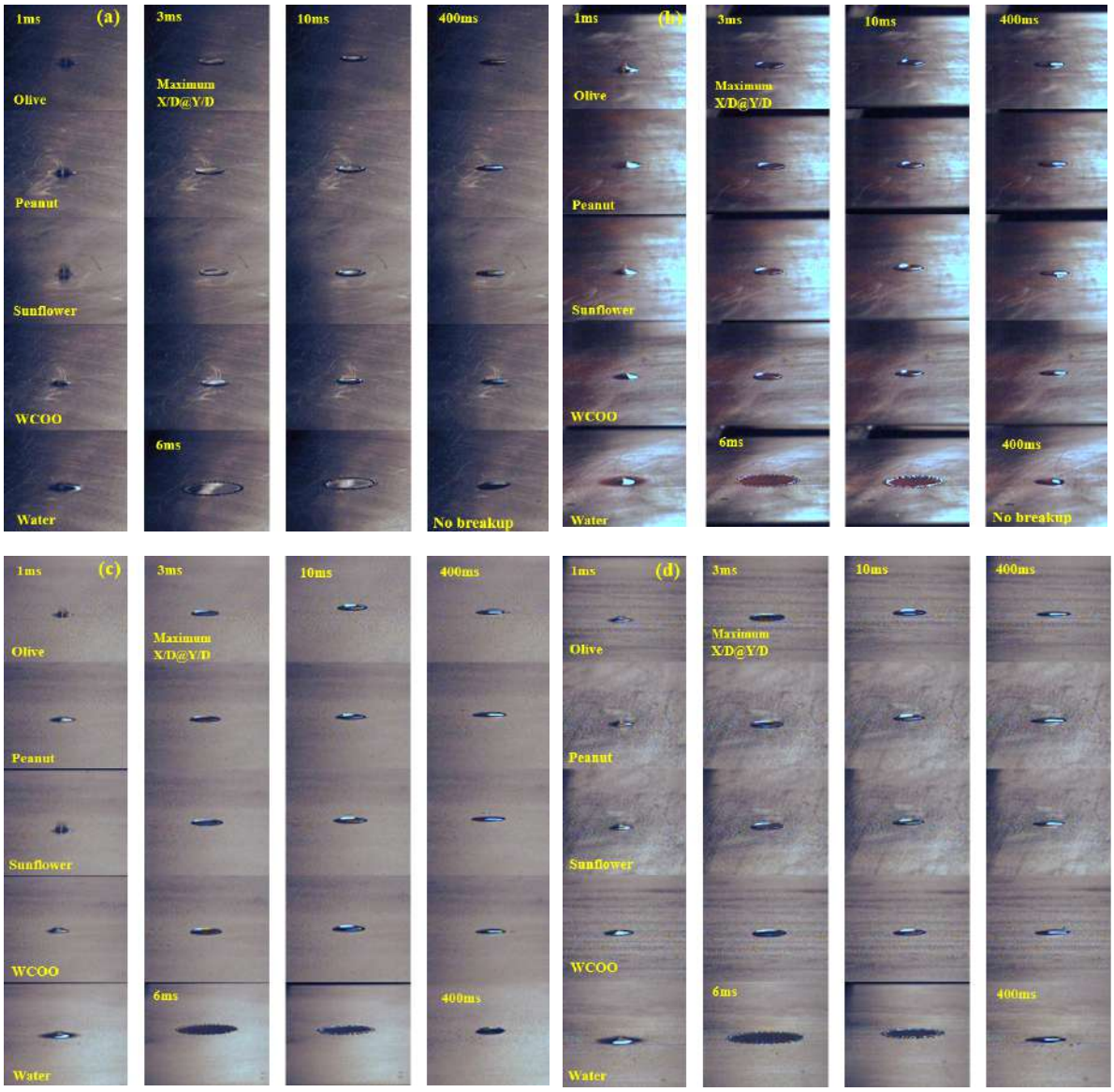

Fig. 4. High-speed images of bio-oils and distilled water droplets at an inclination angle of 5° (a) Ra = 0.5448 µm, aluminum (b) Ra = 0.3488 µm, copper (c) Ra = 1.1728 µm, mild steel, and (d) Ra = 2.2229 µm stainless steel. The droplets were released from a vertical height of 80 cm with an impact velocity of 3.96 m/s, and a high We of approximately 923. Time stamps show first contact (3 ms), intermediate spreading, maximum spreading, and partial retraction

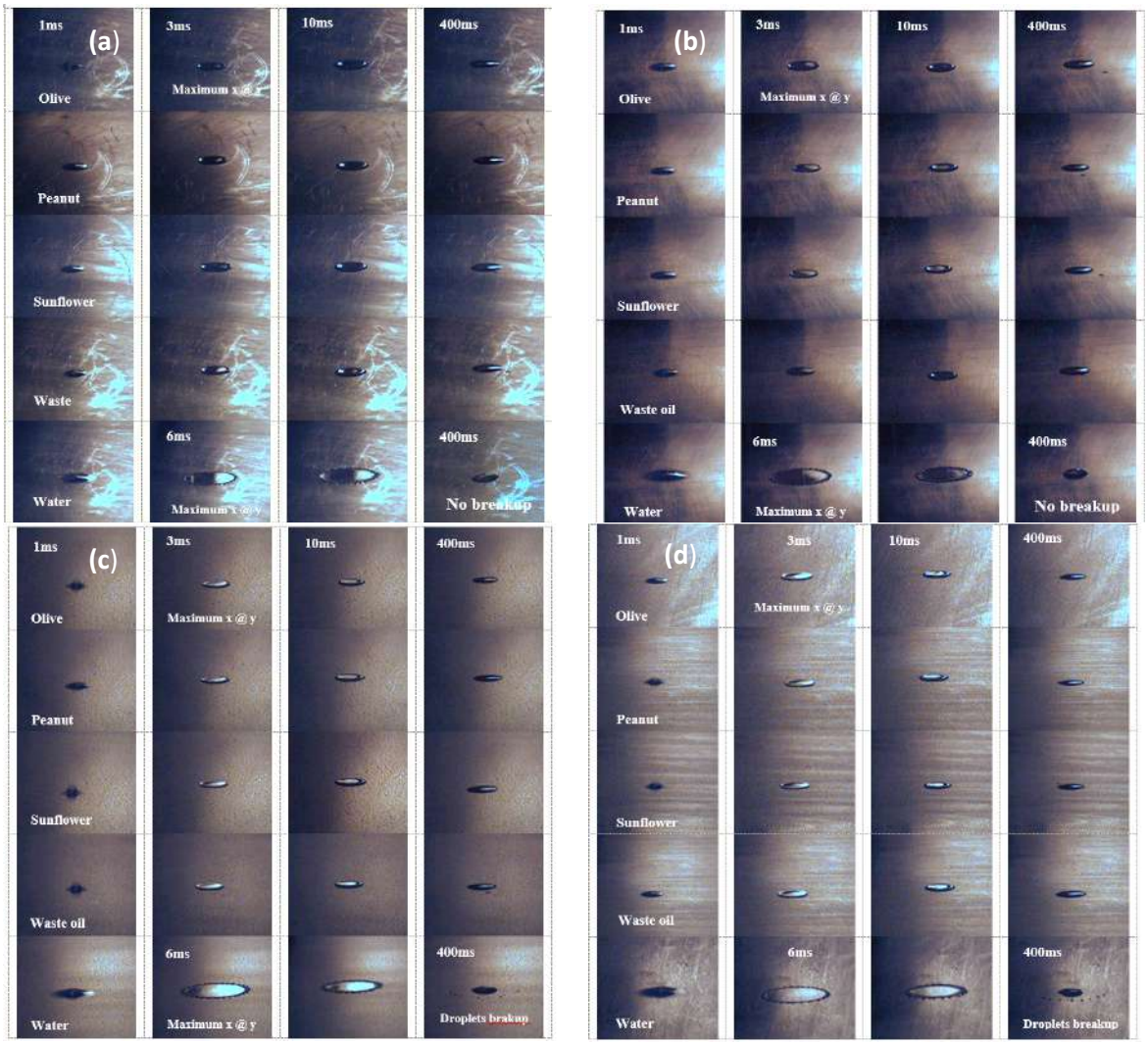

Fig. 5. High-speed images of bio-oils and distilled water droplets at an inclination angle of 10° (a) Ra = 0.5448 µm, aluminum (b) Ra = 0.3488 µm, copper (c) Ra = 1.1728 µm, mild steel, and (d) Ra = 2.2229 µm stainless steel. The droplets were released from a vertical height of 80 cm with an impact velocity of 3.96 m/s, and a high We of approximately 923. Time stamps show first contact (3 ms), intermediate spreading, maximum spreading, and partial retraction

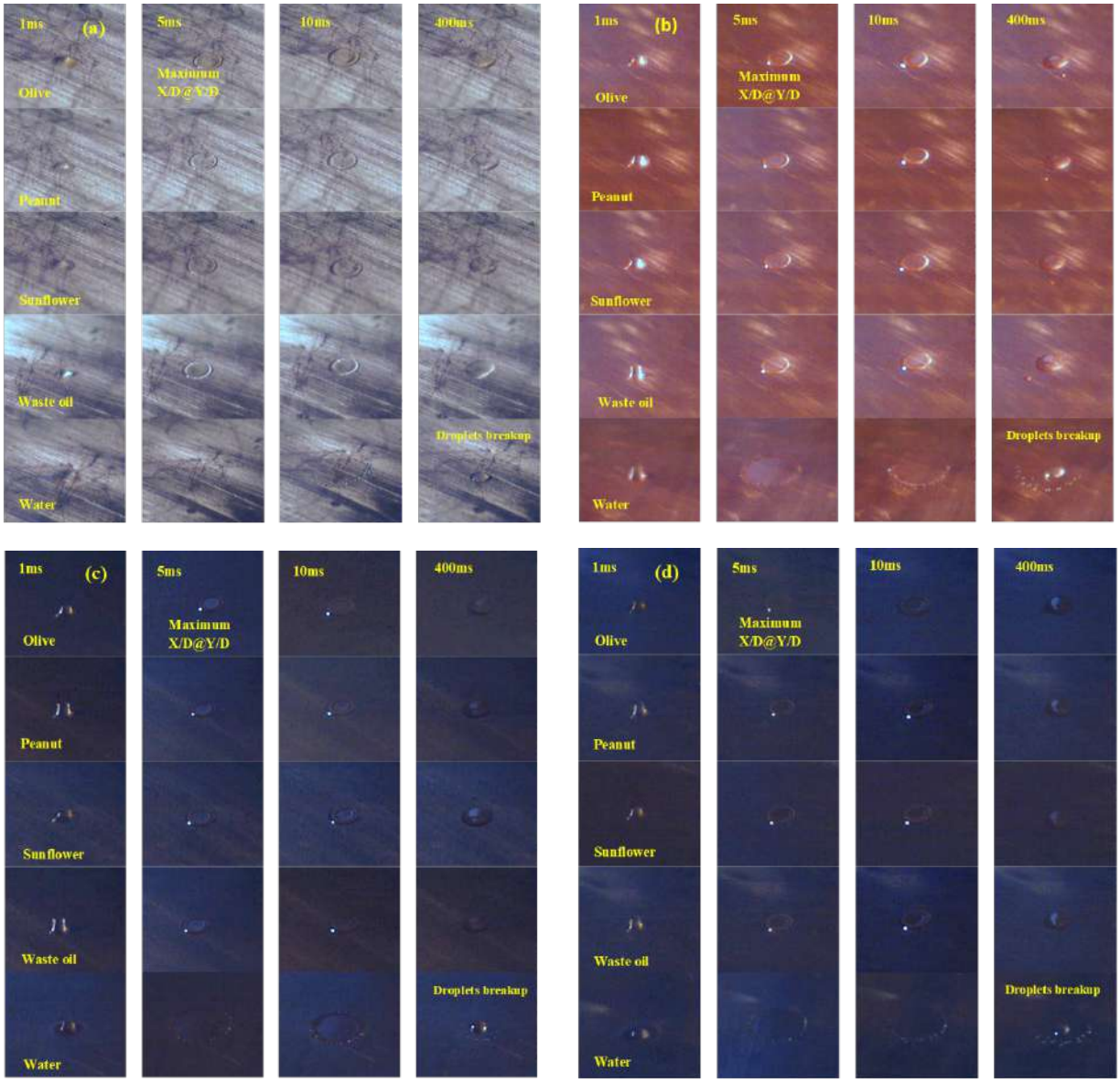

Fig. 6. High-speed images of bio-oils and distilled water droplets at an inclination angle of 30° (a) (Ra = 0.5448 µm), aluminum (b) (Ra = 0.3488µm) copper (c) (Ra = 1.1728µm) mild steel (d) (Ra = 2.2229µm) stainless steel. The droplets were released from a vertical height of 80 cm with an impact velocity of 3.96 m/s, and a high We of approximately 923. Time stamps show first contact (1 ms), intermediate spreading, maximum spreading, and partial retraction

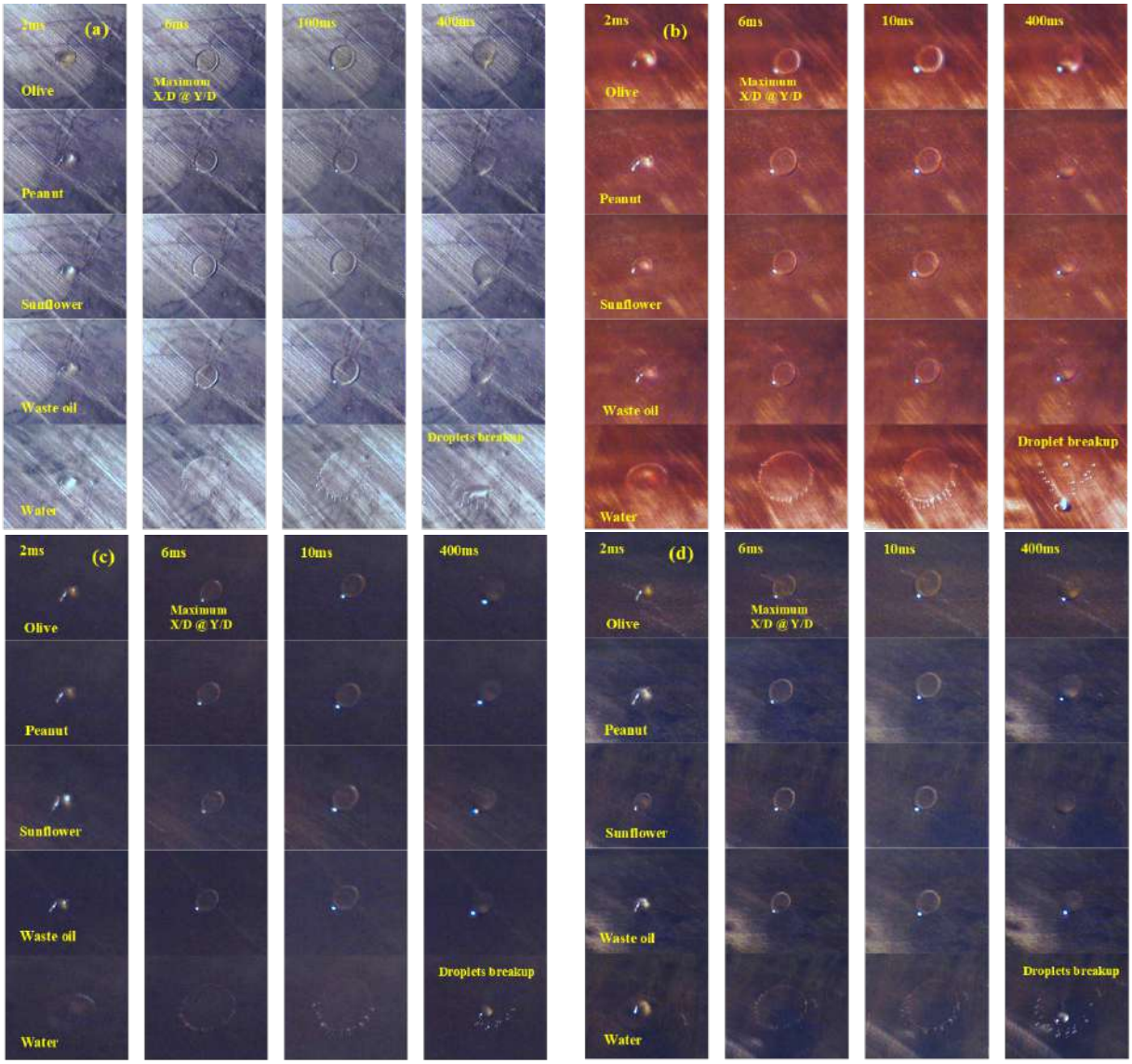

Fig. 7. High-speed images of bio-oils and distilled water droplets at an inclination angle of 45 (a) (Ra = 0.5448 µm), aluminum (b) (Ra = 0.3488µm) copper (c) (Ra = 1.1728µm) mild steel (d) (Ra = 2.2229µm) stainless steel. The droplets were released from a vertical height of 80 cm with an impact velocity of 3.96 m/s, and a high We of approximately 923. Time stamps show first contact (2 ms), intermediate spreading, maximum spreading, and partial retraction

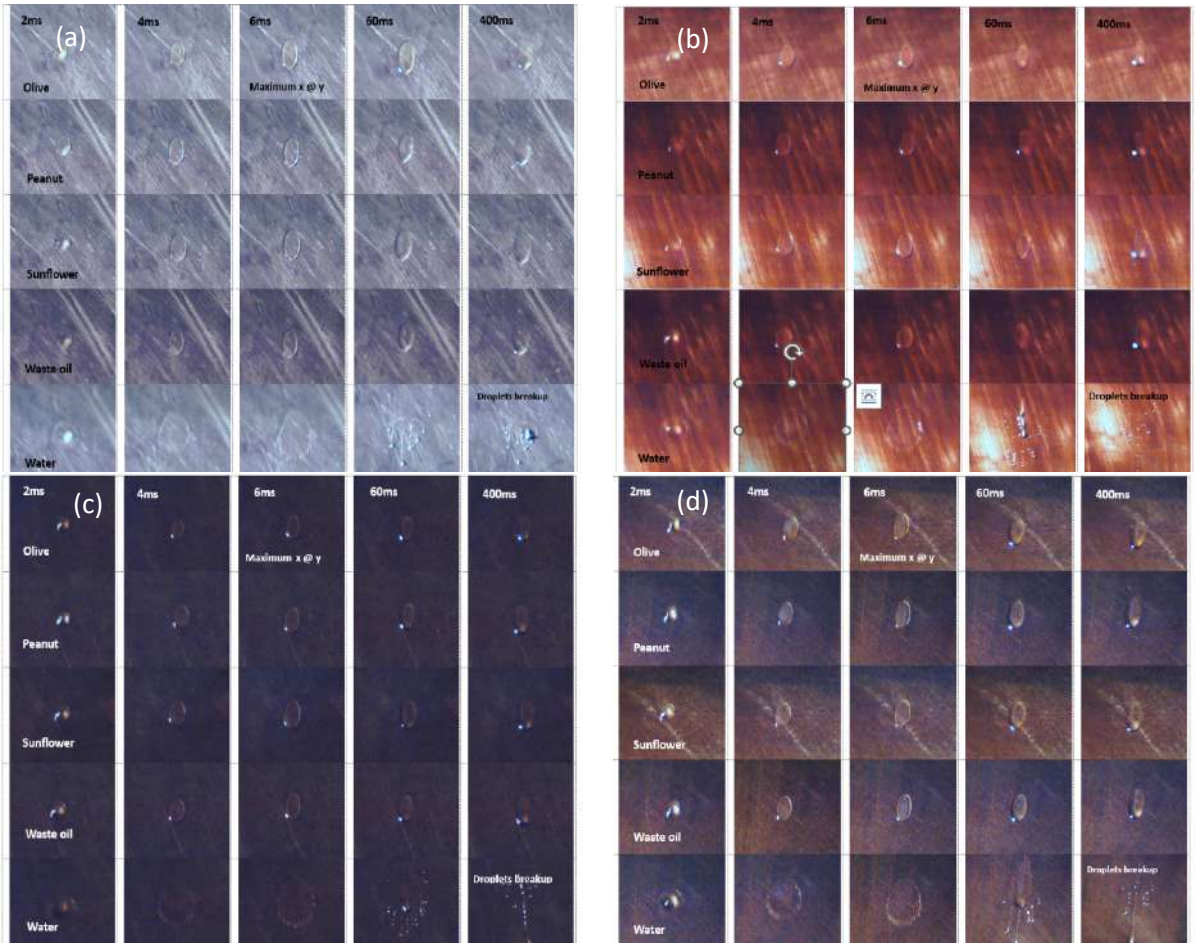

Fig. 8. High-speed images of bio-oils and distilled water droplets at an inclination angle of 60° (a) (Ra = 0.5448 µm), aluminum (b) (Ra = 0.3488µm) copper (c) (Ra = 1.1728µm) mild steel (d) (Ra = 2.2229µm) stainless steel. The droplets were released from 80 cm with a 3.96 m/s impact velocity and a high We of approximately 923. Time stamps show first contact (2 ms), intermediate spreading, maximum spreading, and partial retraction

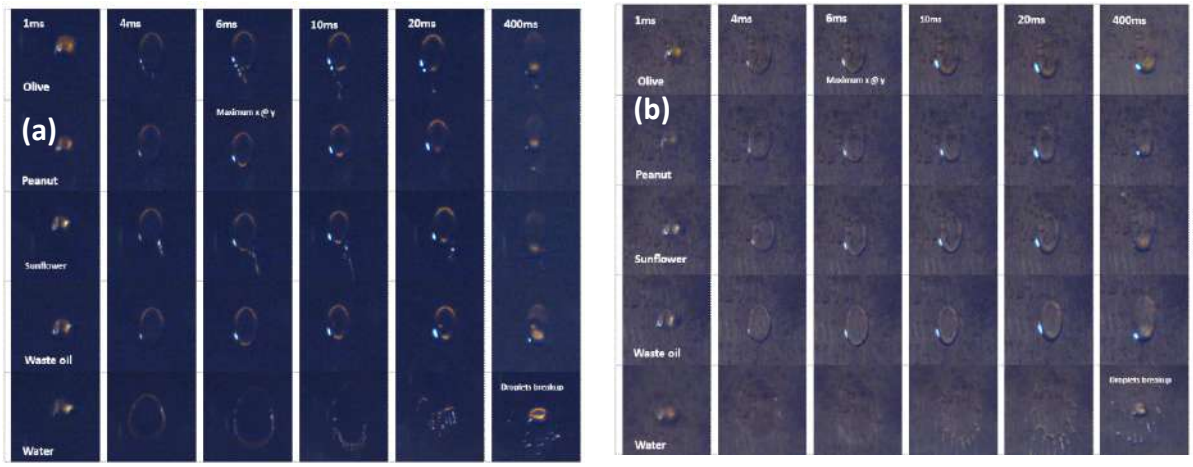

Fig. 9. High-speed images of bio-oil droplets (olive, peanut, sunflower, and waste oil) and distilled water droplets on a controlled roughness (a) (Ra = 0.1019 µm) inclined stainless steel surface angle of 60° and (b) (Ra = 2.2229 µm) inclined stainless steel surface at ambient temperature. The droplets were released from 105 cm with a 4.54 m/s impact velocity and We of approximately 1214. Time stamps show first contact (1 ms), intermediate spreading, maximal spreading, and partial retraction

3.1.1 Weber number effect on spreading

The Weber number was identified as the dominant parameter governing droplet spreading and instability on inclined metallic surfaces because it controls the balance between inertial and surface tension forces. At We ≈ 923 (U_o = 3.96 m/s), droplets of all bio-oils exhibited stable lamella formation with compact footprints even at steep inclinations. The maximum downslope extension remained within Y/D = 4.0–5.0, while streamwise spreading contracted to X/D = 2.5–3.0 at 60°. No splashing or detachment was observed, indicating that viscous damping dominated over inertial stresses for bio-oils. Water, by contrast, was much more sensitive to inertia at the same Weber number. At an inclination angle of 60°, water collapsed downslope with Y/D > 11 and secondary droplet formation, reflecting the lower Ohnesorge number (Oh ≈ 0.0023) of water compared with oils (Oh ≈ 0.12–0.14). These results show that low-viscosity fluids are more prone to inertial destabilization because limited viscous dissipation allows rim instabilities to grow rapidly and generate secondary droplets. To further assess the role of inertia under extreme inclination, additional experiments were conducted at 4.54 m/s (We ≈ 1214) and an inclination angle of 60°. When the impact velocity was increased to U_o = 4.54 m/s (We ≈ 1214) at 60° (Figure 9), inertia amplified downslope spreading and further destabilized the lamellae. On smooth stainless steel (Ra ≈ 0.10 μm), sunflower and olive oil produced crown-like rims with localized splashing, marking the onset of splash for bio-oils. This transition indicates that inertial stresses begin to overcome viscous stabilization at elevated Weber number, particularly on smooth surfaces where contact-line resistance is minimal. In contrast, peanut oil and the waste–olive blend maintained cohesive spreading with Y/D ≈ 5–6 and no rim detachment. On rough stainless steel (Ra ≈ 2.22 μm), all oils completely suppressed splashing and instead formed stable elongated footprints (X/D ≈ 2.6–2.9; Y/D ≈ 4.7–5.1). Water remained highly unstable at elevated Weber number, generating rims that disintegrated into satellite droplets with Y/D approaching 9–10. The quantitative dependence of spreading on Weber number is further illustrated by the maximum Y/D and X/D values for bio-oils and water at all inclination angles. Figure 10 presents the dimensionless spreading evolution at 3 ms on an aluminum surface with Ra = 0.5–0.7 at We = 923. At 5°, all bio-oils spread slowly and symmetrically in both directions (X/D ≈ 3–3.7, Y/D ≈ 0.5–0.7), whereas water spread more extensively (X/D ≈ 6.2–6.4, Y/D ≈ 1.4). As the inclination angle increased from 10° to 60°, the maximum X/D remained relatively stable or slightly decreased, whereas Y/D increased significantly, indicating progressively asymmetric spreading driven by enhanced downslope momentum. Figure 11 shows the corresponding results for a copper surface with Ra = 0.34–0.37 at the same Weber number. The maximum spreading exhibited slightly higher Y/D values, while the X/D ratio remained nearly constant, suggesting that the copper surface promoted preferential spreading in the downslope direction. For mild steel surfaces (Figure 12) with Ra = 0.95–1.17, both X/D and Y/D showed lower maximum spreading compared with aluminum and copper across all angles, indicating greater suppression of lamella expansion. Figure 13 presents the results for stainless steel surfaces with Ra = 1.90–2.22, where both X/D and Y/D were further reduced, demonstrating that increased surface roughness increasingly restricted spreading in both directions. Collectively, these results indicate that increasing surface roughness progressively suppresses droplet spreading by enhancing viscous dissipation and contact-line pinning at the solid–liquid interface.

While Y/D increased sharply for water at We = 1214, accompanied by rim breakup and satellite droplet formation, bio-oils showed only modest growth in spreading. X/D exhibited a slight reduction with increasing Weber number, indicating contraction of streamwise spreading due to enhanced downslope momentum (Figure 14). These findings demonstrate that the influence of surface roughness is strongly dependent on the inertial regime. At moderate Weber number, roughness exerts only a minor influence because inertial forces are insufficient to strongly activate surface

irregularities. However, at elevated Weber number, increased contact-line motion amplifies the interaction between the lamella and surface topography, allowing roughness-induced pinning to effectively suppress rim instability and splashing. Collectively, these results highlight the competing roles of inertia, viscosity, and surface interaction during droplet impact on inclined metallic surfaces. Increasing Weber number intensifies spreading asymmetry and promotes rim instability, particularly in low-viscosity fluids such as water. In contrast, bio-oils maintain greater spreading stability due to enhanced viscous dissipation. Surface roughness further modifies this balance by enhancing contact-line pinning, which becomes increasingly effective at high inertia where instability would otherwise dominate. These findings establish a unified physical interpretation of splash onset and suppression mechanisms for bio-oils on inclined metallic substrates.

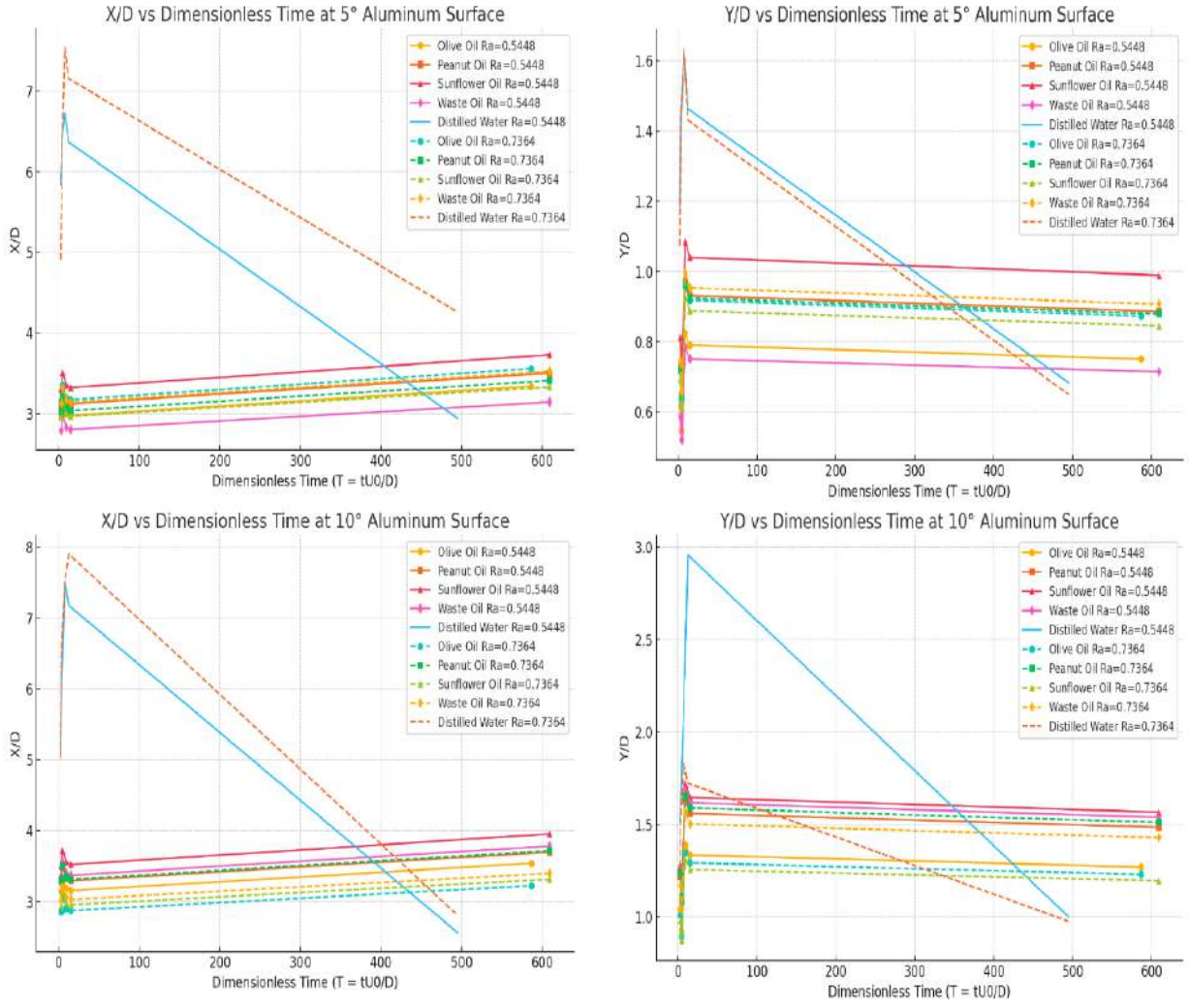

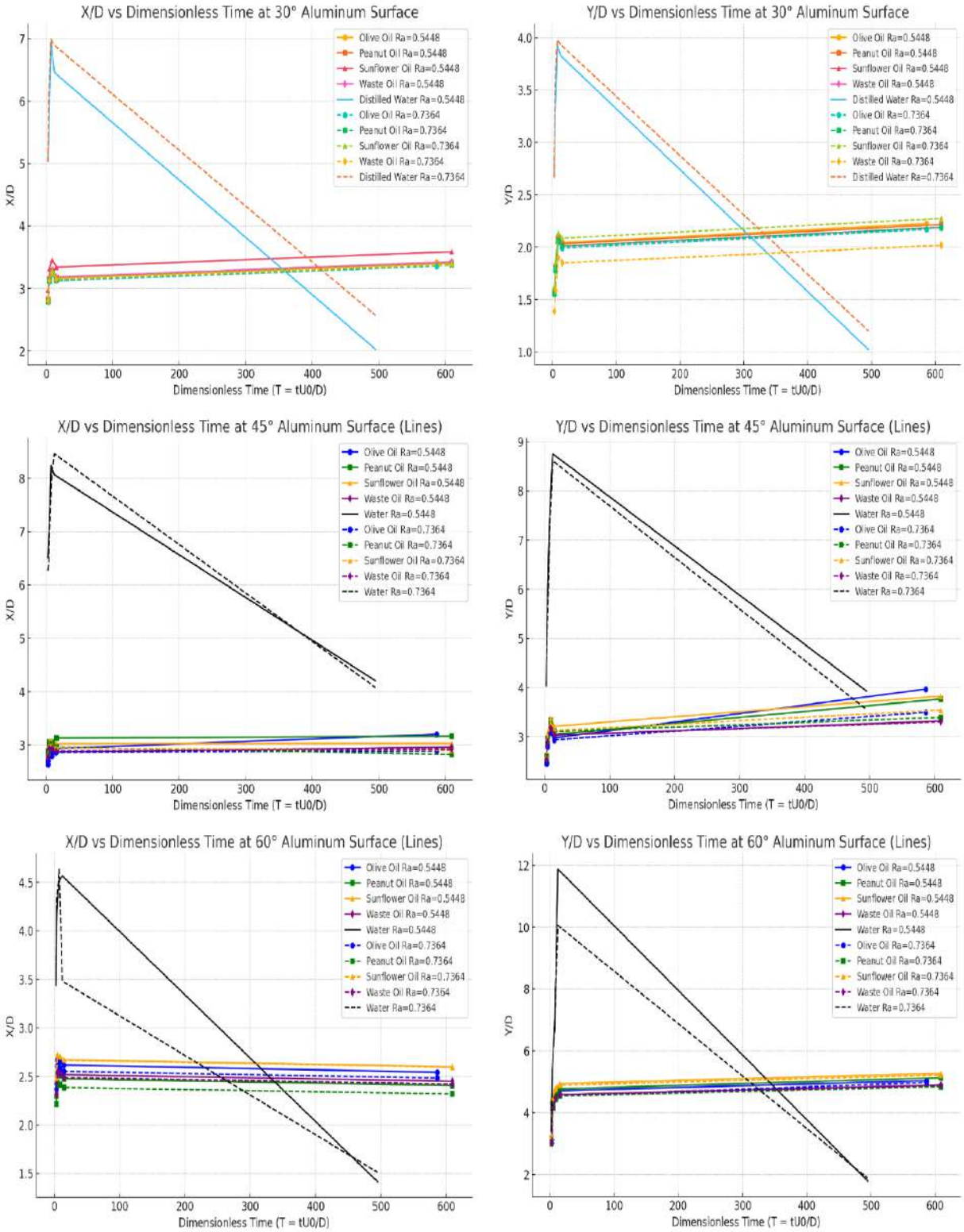

Fig. 10. X/D and Y/D at inclination angles of 5º, 10º, 30º, 45º, and 60º, under constant height, velocity, and We on an aluminum surface with two surface roughness values (Ra = 0.5448 µm and Ra = 0.7364 µm)

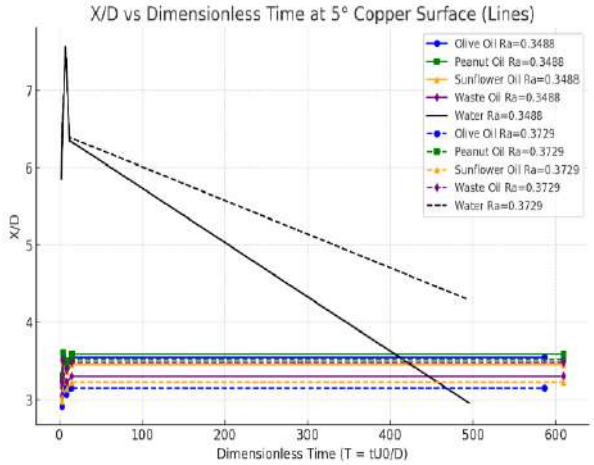
X/D vs Dimensionless Time at 5° Copper Surface (Lines)
X/D
Dimensionless Time (T = tU0/D)
Olive Oil Ra=0.3488
Peanut Oil Ra=0.3488
Sunflower Oil Ra=0.3488
Waste Oil Ra=0.3488
Water Ra=0.3488
Olive Oil Ra=0.3729
Peanut Oil Ra=0.3729
Sunflower Oil Ra=0.3729
Waste Oil Ra=0.3729
Water Ra=0.3729

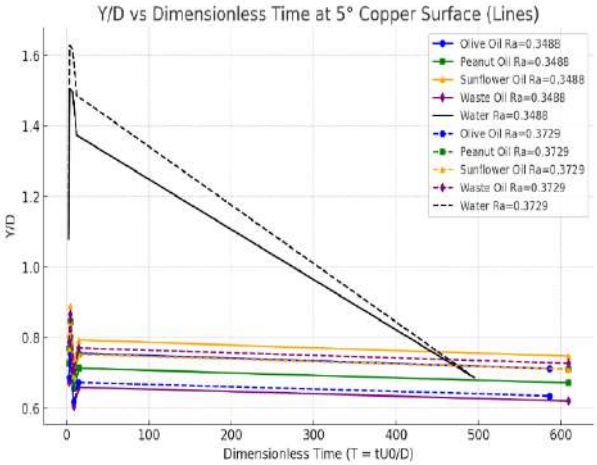
Y/D vs Dimensionless Time at 5° Copper Surface (Lines)
Y/D
Dimensionless Time (T = tU0/D)
Olive Oil Ra=0.3488
Peanut Oil Ra=0.3488
Sunflower Oil Ra=0.3488
Waste Oil Ra=0.3488
Water Ra=0.3488
Olive Oil Ra=0.3729
Peanut Oil Ra=0.3729
Sunflower Oil Ra=0.3729
Waste Oil Ra=0.3729
Water Ra=0.3729

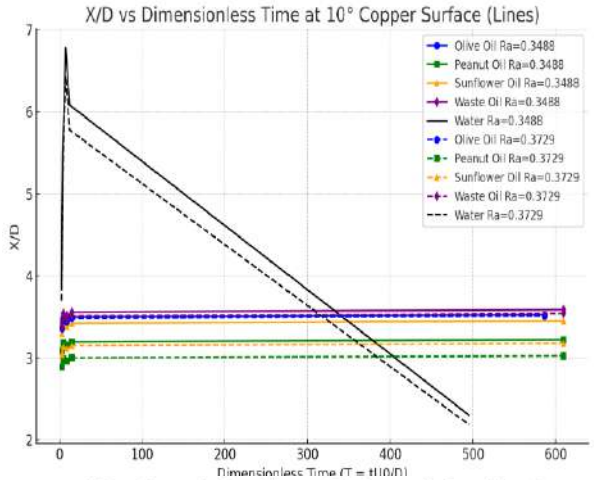
X/D vs Dimensionless Time at 10° Copper Surface (Lines)
X/D
Olive Oil Ra=0.3488
Peanut Oil Ra=0.3488
Sunflower Oil Ra=0.3488
Waste Oil Ra=0.3488
Water Ra=0.3488
Olive Oil Ra=0.3729
Peanut Oil Ra=0.3729
Sunflower Oil Ra=0.3729
Waste Oil Ra=0.3729
Water Ra=0.3729

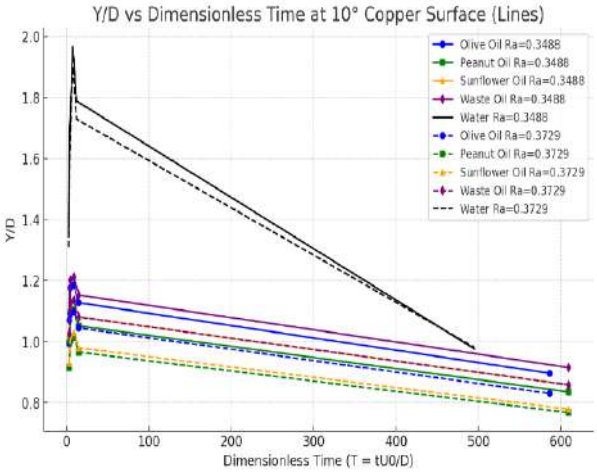
Y/D vs Dimensionless Time at 10° Copper Surface (Lines)
Y/D
Dimensionless Time (T = tU0/D)
Olive Oil Ra=0.3488
Peanut Oil Ra=0.3488
Sunflower Oil Ra=0.3488
Waste Oil Ra=0.3488
Water Ra=0.3488
Olive Oil Ra=0.3729
Peanut Oil Ra=0.3729
Sunflower Oil Ra=0.3729
Waste Oil Ra=0.3729
Water Ra=0.3729

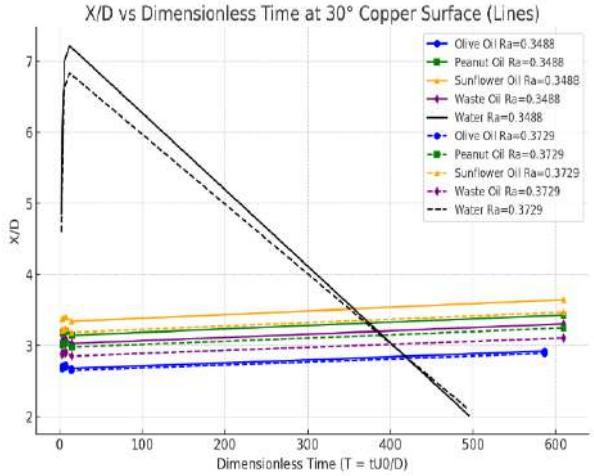
X/D vs Dimensionless Time at 30° Copper Surface (Lines)
X/D
Dimensionless Time (T = tU0/D)
Olive Oil Ra=0.3488
Peanut Oil Ra=0.3488
Sunflower Oil Ra=0.3488
Waste Oil Ra=0.3488
Water Ra=0.3488
Olive Oil Ra=0.3729
Peanut Oil Ra=0.3729
Sunflower Oil Ra=0.3729
Waste Oil Ra=0.3729
Water Ra=0.3729

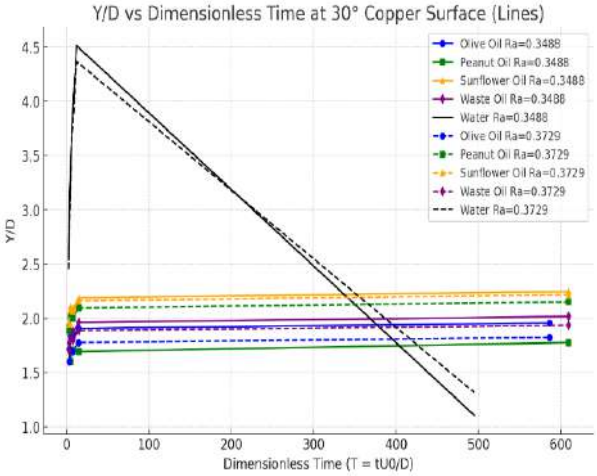
Y/D vs Dimensionless Time at 30° Copper Surface (Lines)
Y/D
Dimensionless Time (T = tU0/D)
Olive Oil Ra=0.3488
Peanut Oil Ra=0.3488
Sunflower Oil Ra=0.3488
Waste Oil Ra=0.3488
Water Ra=0.3488
Olive Oil Ra=0.3729
Peanut Oil Ra=0.3729
Sunflower Oil Ra=0.3729
Waste Oil Ra=0.3729
Water Ra=0.3729

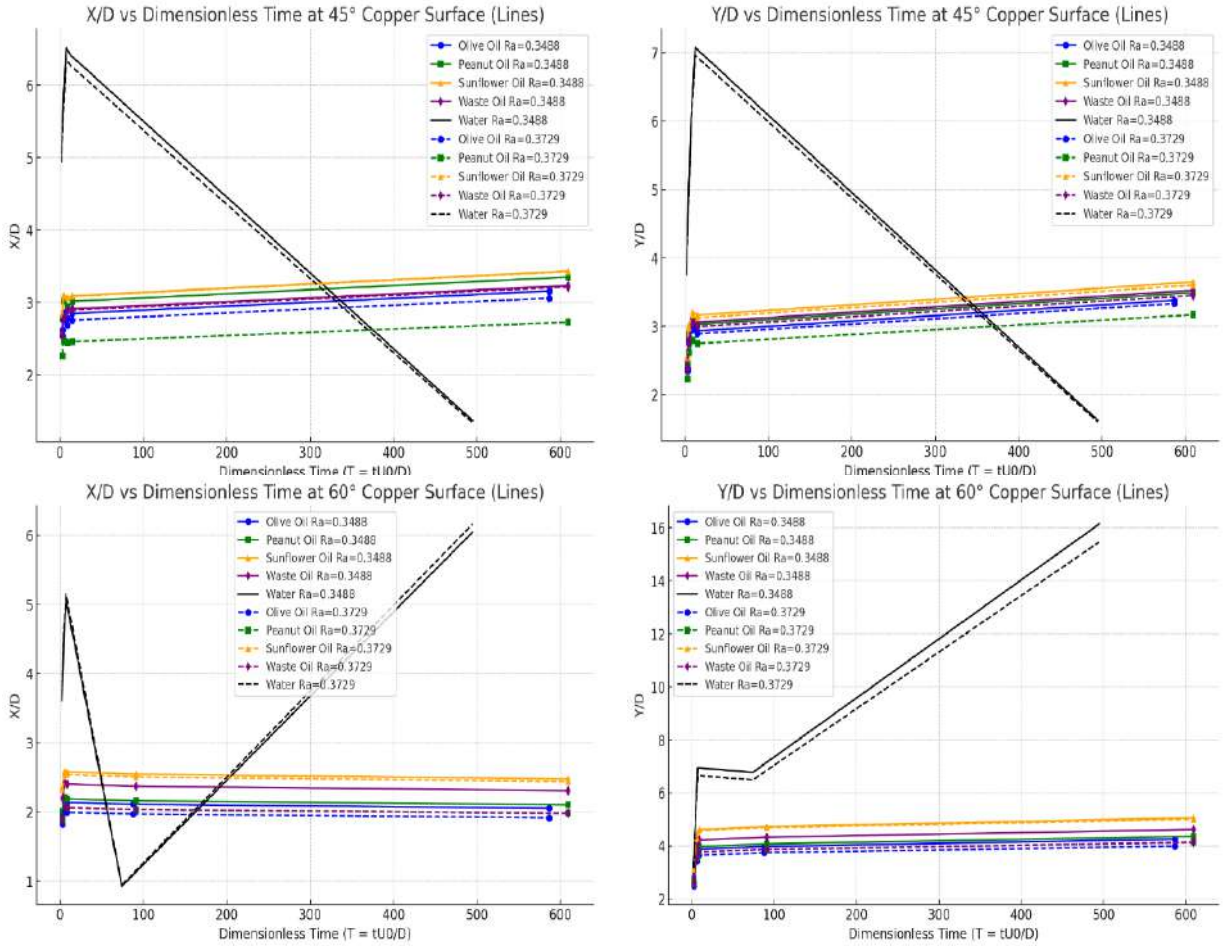

Fig. 11. X/D and Y/D at inclination angles of 5º, 10º, 30º,45º, and 60º, under constant height, velocity, and We on a copper surface with two surface roughness effects (Ra = 0.3488µm and Ra = 0.3729µm)

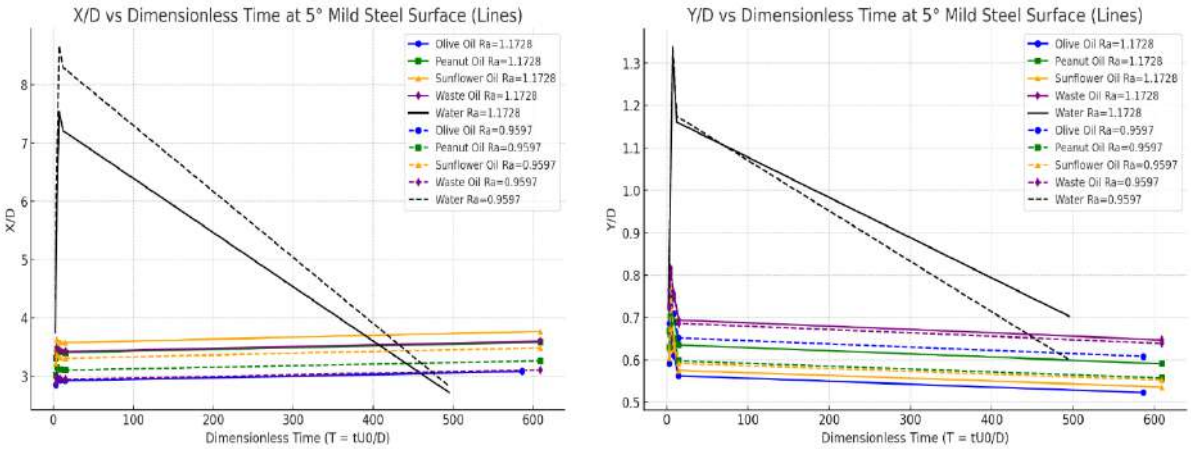

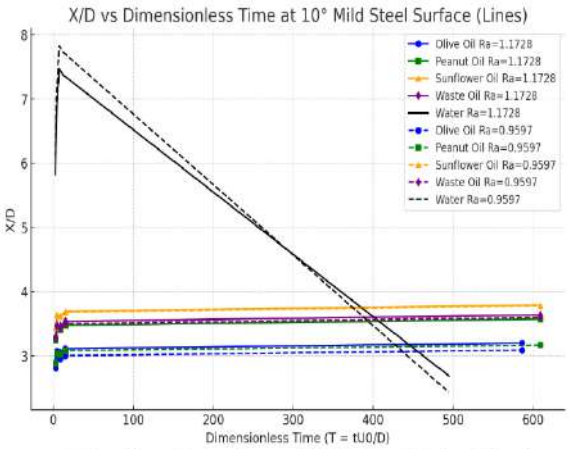
X/D vs Dimensionless Time at 10° Mild Steel Surface (Lines)
X/D
Dimensionless Time (T = tU0/D)
Olive Oil Ra=1.1728
Peanut Oil Ra=1.1728
Sunflower Oil Ra=1.1728
Waste Oil Ra=1.1728
Water Ra=1.1728
Olive Oil Ra=0.9597
Peanut Oil Ra=0.9597
Sunflower Oil Ra=0.9597
Waste Oil Ra=0.9597
Water Ra=0.9597

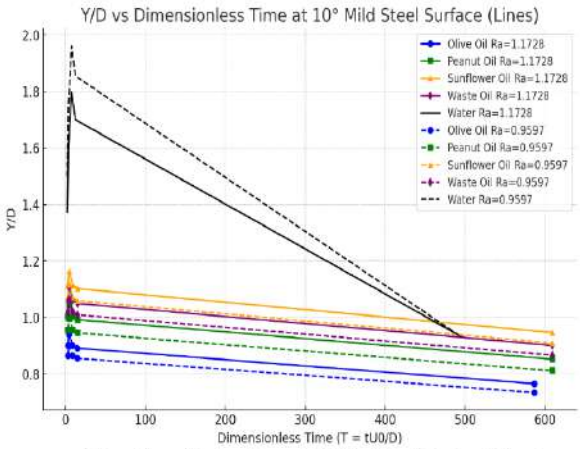
Y/D vs Dimensionless Time at 10° Mild Steel Surface (Lines)
Y/D
Dimensionless Time (T = tU0/D)
Olive Oil Ra=1.1728
Peanut Oil Ra=1.1728
Sunflower Oil Ra=1.1728
Waste Oil Ra=1.1728
Water Ra=1.1728
Olive Oil Ra=0.9597
Peanut Oil Ra=0.9597
Sunflower Oil Ra=0.9597
Waste Oil Ra=0.9597
Water Ra=0.9597

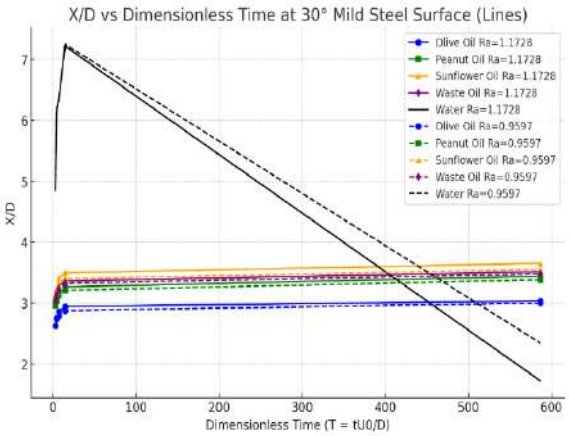
X/D vs Dimensionless Time at 30° Mild Steel Surface (Lines)
X/D
Dimensionless Time (T = tU0/D)
Olive Oil Ra=1.1728
Peanut Oil Ra=1.1728
Sunflower Oil Ra=1.1728
Waste Oil Ra=1.1728
Water Ra=1.1728
Olive Oil Ra=0.9597
Peanut Oil Ra=0.9597
Sunflower Oil Ra=0.9597
Waste Oil Ra=0.9597
Water Ra=0.9597

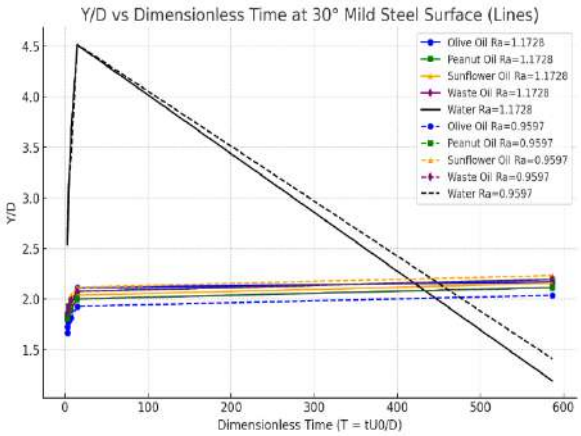
Y/D vs Dimensionless Time at 30° Mild Steel Surface (Lines)
Y/D
Dimensionless Time (T = tU0/D)
Olive Oil Ra=1.1728
Peanut Oil Ra=1.1728
Sunflower Oil Ra=1.1728
Waste Oil Ra=1.1728
Water Ra=1.1728
Olive Oil Ra=0.9597
Peanut Oil Ra=0.9597
Sunflower Oil Ra=0.9597
Waste Oil Ra=0.9597
Water Ra=0.9597

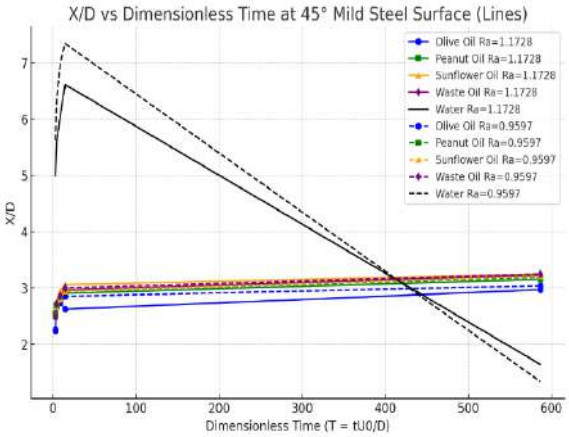
X/D vs Dimensionless Time at 45° Mild Steel Surface (Lines)
X/D
Dimensionless Time (T = tU0/D)
Olive Oil Ra=1.1728
Peanut Oil Ra=1.1728
Sunflower Oil Ra=1.1728
Waste Oil Ra=1.1728
Water Ra=1.1728
Olive Oil Ra=0.9597
Peanut Oil Ra=0.9597
Sunflower Oil Ra=0.9597
Waste Oil Ra=0.9597
Water Ra=0.9597

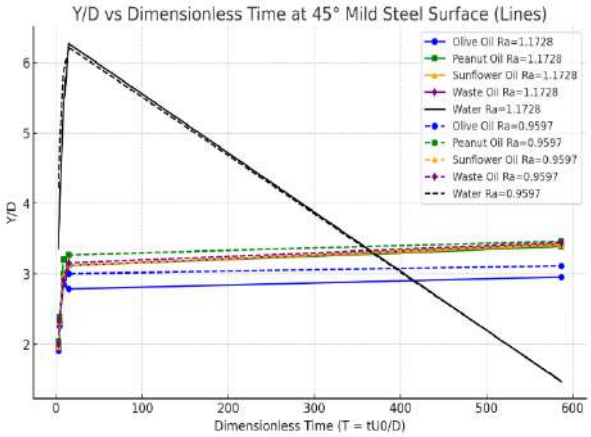
Y/D vs Dimensionless Time at 45° Mild Steel Surface (Lines)
Y/D
Dimensionless Time (T = tU0/D)
Olive Oil Ra=1.1728
Peanut Oil Ra=1.1728
Sunflower Oil Ra=1.1728
Waste Oil Ra=1.1728
Water Ra=1.1728
Olive Oil Ra=0.9597
Peanut Oil Ra=0.9597
Sunflower Oil Ra=0.9597
Waste Oil Ra=0.9597
Water Ra=0.9597

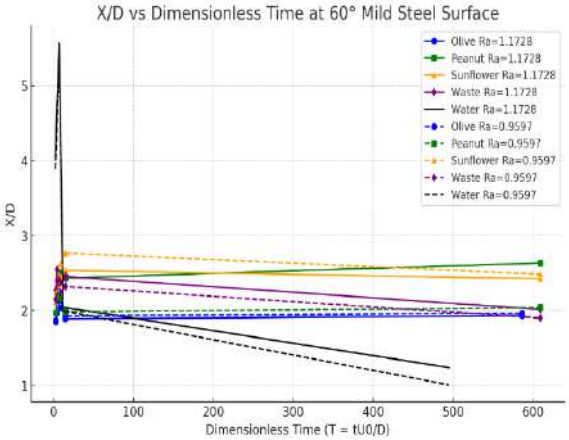
X/D vs Dimensionless Time at 60° Mild Steel Surface
X/D
Dimensionless Time (T = tU0/D)
Olive Ra=1.1728
Peanut Ra=1.1728
Sunflower Ra=1.1728
Waste Ra=1.1728
Water Ra=1.1728
Olive Ra=0.9597
Peanut Ra=0.9597
Sunflower Ra=0.9597
Waste Ra=0.9597
Water Ra=0.9597

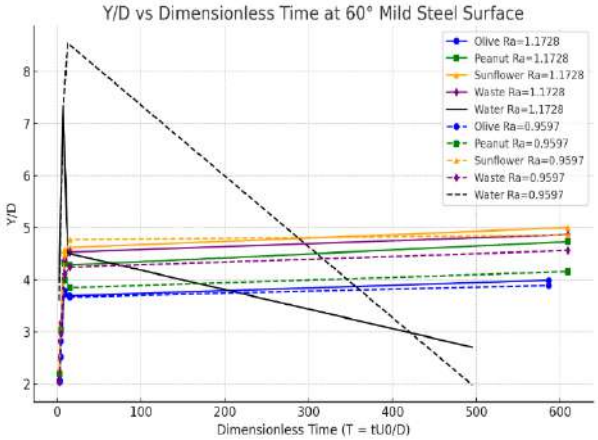
Y/D vs Dimensionless Time at 60° Mild Steel Surface
Y/D
Dimensionless Time (T = tU0/D)
Olive Ra=1.1728
Peanut Ra=1.1728
Sunflower Ra=1.1728
Waste Ra=1.1728
Water Ra=1.1728
Olive Ra=0.9597
Peanut Ra=0.9597
Sunflower Ra=0.9597
Waste Ra=0.9597
Water Ra=0.9597

Fig. 12. X/D and Y/D at inclination angles of 5º, 10º, 30º, 45º, and 60º, under constant height, velocity, and We on a mild steel surface with two surface roughness effects (Ra = 1.1728µm and Ra = 0.9597µm)

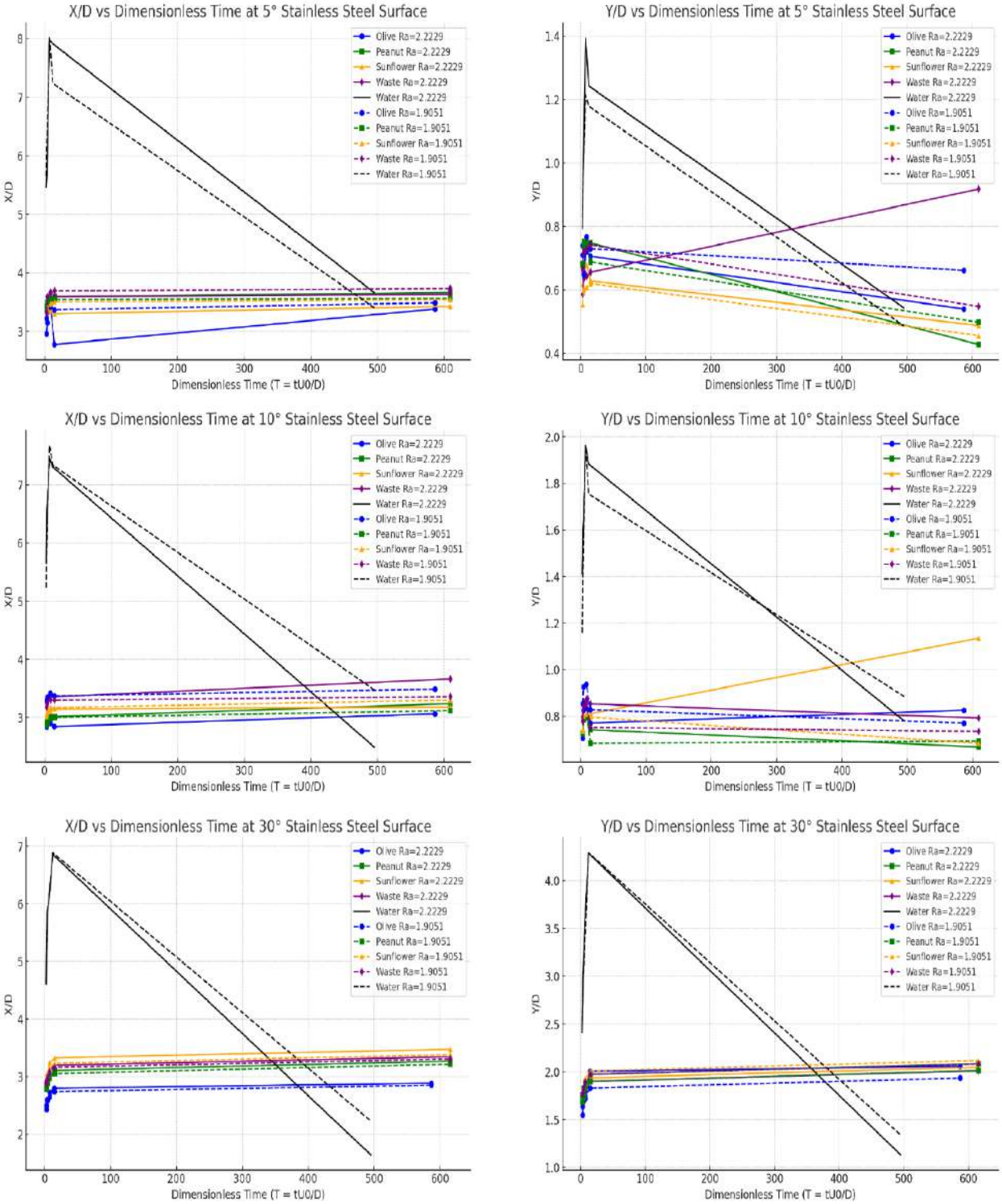

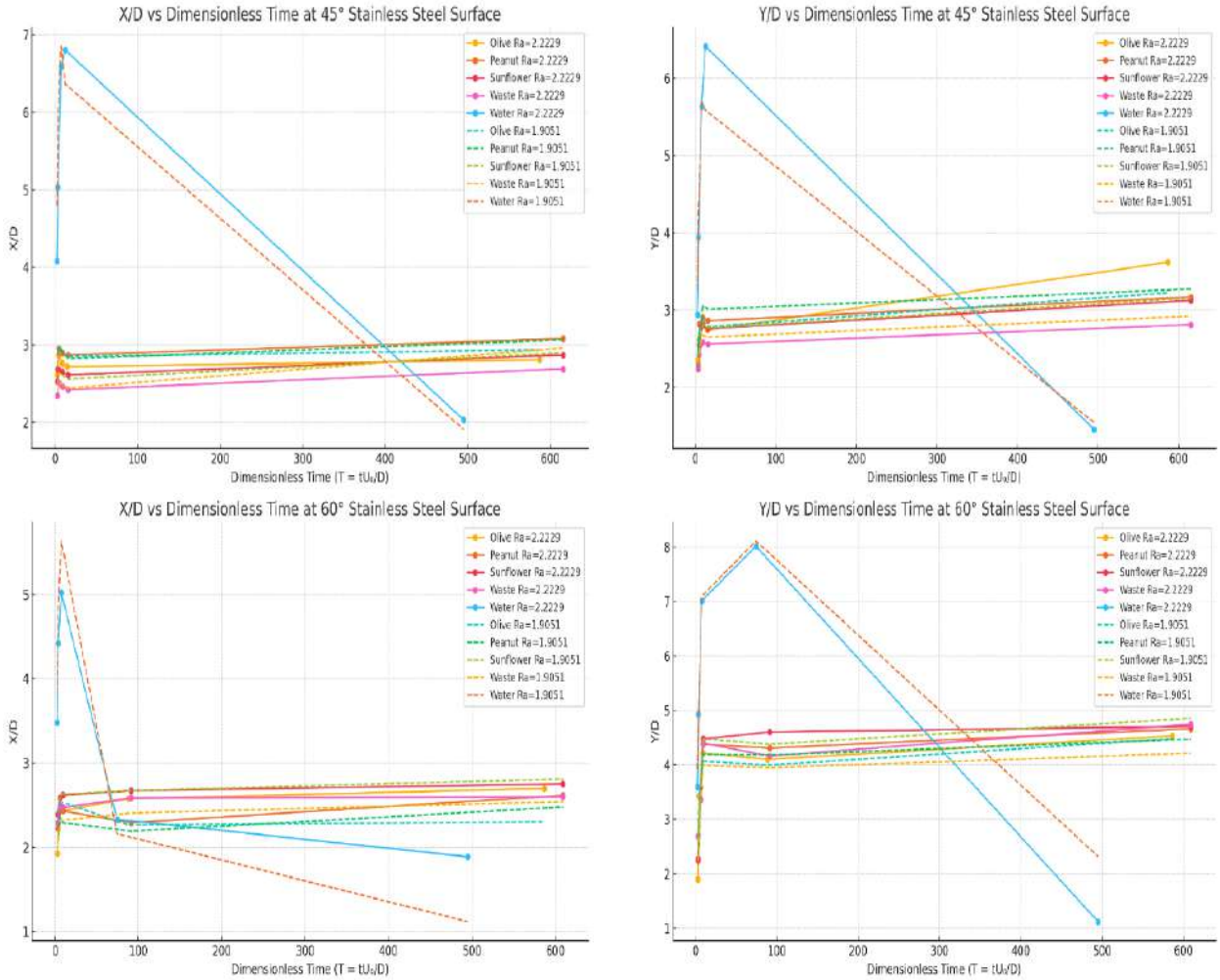

Fig. 13. X/D and Y/D at inclination angles of 5º, 10º, 30º, 45º, and 60º, under constant height, velocity, and We on a stainless-steel surface with two surface roughness effects (Ra = 2.2229µm and Ra = 1.9051µm)

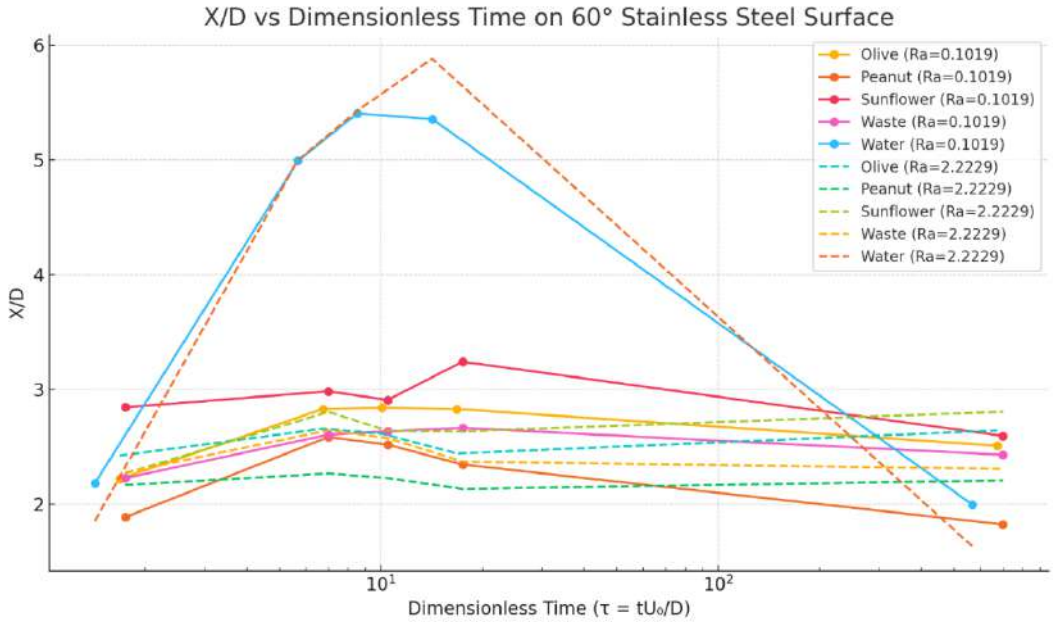

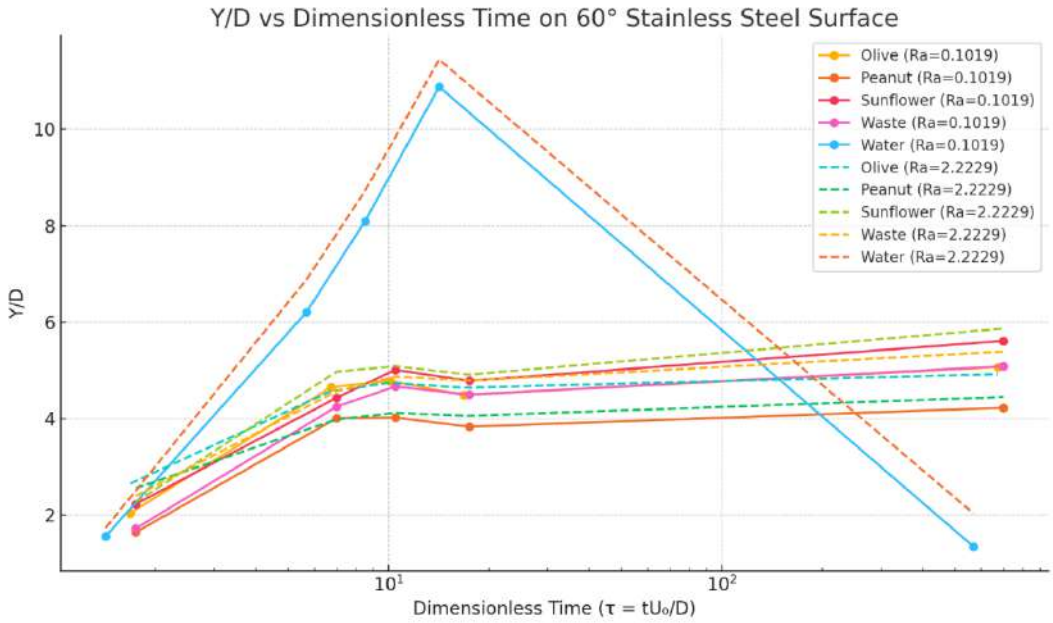

Fig. 14. X/D and Y/D for stainless-steel surfaces at an inclination angle of 60° at high We (U_o = 4.54 m/s). Results are compared between a smooth surface (Ra ≈ 0.10 µm) and a rough surface (Ra ≈ 2.22 µm) to highlight the role of surface roughness in suppressing or promoting splash behavior

3.1.2 Roughness–angle interaction and lamella pinning

The influence of surface roughness on droplet spreading and lamella stability was systematically evaluated at moderate Weber number (We = 923, U_o = 3.96 m/s) across four metallic substrates (aluminum, copper, mild steel, and stainless steel) over inclination angles ranging from 5° to 60°. An additional high-inertia condition (We = 1214, U_o = 4.54 m/s) was investigated exclusively on stainless steel at 60° to examine the onset of splash under smooth and rough surface conditions. The results indicate that the role of surface roughness is strongly dependent on the inertial regime and becomes increasingly important at elevated Weber number. At We = 923, the influence of surface roughness was generally secondary compared with the effects of inclination angle and fluid viscosity. On aluminum and copper surfaces, the difference between smoother surfaces (Ra ≈ 0.35–0.55 µm) and rougher surfaces (Ra ≈ 0.37–0.73 µm) produced only minor variations in spreading, with ΔX/D and ΔY/D typically remaining below 0.2 across all inclinations. Bio-oils remained compact (X/D ≈ 2.5–3.9; Y/D ≈ 0.8–5.0) and splash-free under both roughness conditions, whereas water spread more extensively (X/D approaching 8.0 and Y/D exceeding 11 at 60°), accompanied by rim breakup at steep inclinations regardless of surface roughness. These findings indicate that, at moderate Weber number, inertial forces are insufficient to strongly activate surface irregularities, and droplet behaviour is governed primarily by inertial–capillary balance and gravitational asymmetry. On mild steel surfaces (Ra ≈ 0.96 and 1.17 µm), roughness effects became slightly more pronounced. Bio-oils exhibited marginal increases in Y/D on the rougher surface at intermediate inclinations (30°–45°) while remaining splash-free. Water displayed somewhat greater spreading on the rougher surface at shallow angles but still fragmented at 60°. On stainless steel, where the roughness span was larger (Ra ≈ 0.10 µm, 1.90 µm, and 2.22 µm), bio-oils again remained highly stable on both smooth and rough substrates, with X/D ≈ 2.6–3.6 and Y/D ≈ 0.8–5.0 across all inclination angles. Water showed slightly enhanced spreading at shallow inclinations on rougher stainless steel, but at 45°–60°, both smooth and rough surfaces produced similar outcomes characterized by strong downslope elongation and rim breakup with satellite droplet formation. Collectively, these results demonstrate

that roughness exerts only a limited influence at moderate Weber number because the available inertial energy is insufficient to fully amplify contact-line disturbances and surface-induced instabilities. At We = 1214 and an inclination angle of 60° on stainless steel, the role of roughness became substantially more significant. On smooth stainless steel (Ra ≈ 0.10 µm), sunflower and olive oil droplets developed unstable rims and localized splashing, producing crown-like structures and small satellite droplets that marked the first splash events observed for bio-oils. This transition indicates that increased inertial stresses begin to overcome viscous stabilization on smooth surfaces where contact-line resistance is minimal. In contrast, on rough stainless steel (Ra ≈ 2.22 µm), all oils remained cohesive with compact footprints (X/D ≈ 2.6–2.9; Y/D ≈ 4.7–5.1), closely resembling the stable spreading behaviour observed at We = 923. Water remained highly unstable under both roughness conditions, generating severe rim breakup and satellite droplet formation with Y/D ≈ 9–10. These findings demonstrate that the influence of surface roughness is strongly regime-dependent. At moderate Weber number, roughness plays only a secondary role relative to inclination angle and fluid viscosity because inertial forces are insufficient to strongly activate surface topography. However, at elevated Weber number, increased contact-line motion amplifies the interaction between the lamella and the substrate, allowing roughness-induced pinning to effectively suppress instability and delay splash onset. Consequently, surface roughness acts as a stabilizing mechanism at high inertia by dissipating kinetic energy and restricting lamella motion, particularly for high-viscosity bio-oils.

3.1.3 Comparison between water and bio-oils

A direct comparison of water and bio-oils underscores the essential influence of fluid characteristics on droplet movements on inclined surfaces. Water, characterized by its low viscosity (≈ 1 mPa·s) and elevated surface tension (≈ 0.072 N/m), exhibited a strong response to both inclination and inertia. At We = 923 (U_o = 3.96 m/s), water consistently generated larger footprints than oils, achieving X/D ≈ 7.0–8.0 and Y/D > 11 at 60°, accompanied by rim thinning and secondary droplet production. Bio-oils, by contrast, formed compact and cohesive lamellae with X/D ratios of around 2.5–3.9 and Y/D ratios of approximately 0.8–5.0, remaining splash-free throughout all metals and surface roughness levels. At higher inertia (We = 1214, U_o = 4.54 m/s), tested at 60° on stainless steel, the contrast became sharper. Water rims destabilized, producing violent splashing and satellite droplets on both smooth and rough surfaces. Among the oils, sunflower and olive oil splashed only on smooth stainless (Ra ≈ 0.10 µm), while peanut oil and the waste olive blend remained stable. On rough stainless (Ra ≈ 2.22 µm), all oils resisted splashing, showing that viscosity coupled with pinning can fully suppress instabilities at Weber numbers beyond 1200. The low Ohnesorge number of water (≈ 0.0023) facilitates inertia-dominated spreading, elongation, and fragmentation, while oils with an Ohnesorge number of approximately 0.12–0.14 maintained pinned, asymmetric spreading without catastrophic breakage. The inclination angle predominantly influences spreading asymmetry: at low slopes, both water and oil spread almost symmetrically; however, at steep angles, water becomes destabilized with Y/D > 11, while oils stay concentrated and free from splashing. Surface roughness is of secondary importance for modest We, but with elevated inertia, it becomes critical, as rough stainless steel (Ra = 2.22 µm) mitigates splashing and maintains stable lamellae throughout all oils. These results have practical implications for droplet control on inclined metallic surfaces. When stable and splash-free deposition is required, higher-viscosity fluids and rougher metallic surfaces are preferred because they enhance contact-line pinning and suppress rim breakup, particularly at high inertia. In contrast, smoother surfaces promote greater lamella spreading but may also increase the likelihood of splash initiation, especially for low-viscosity liquids such as water under high Weber

number conditions. Lower inclination angles favour symmetric spreading and more uniform coverage, whereas steeper angles amplify downslope asymmetry and can lead to uneven deposition. Therefore, for applications requiring uniform coating or efficient cooling, moderate inclination angles are preferable. Conversely, controlled asymmetry induced by higher inclination may be advantageous where directional transport or targeted deposition is desired. Overall, jointly tuning fluid viscosity, surface roughness, and inclination angle provides a practical framework for optimizing droplet–surface interactions in engineering systems, particularly those involving bio-oil fuels and complex surface geometries.

4. Conclusions

This study investigated the impact behaviour of bio-oil droplets on inclined metallic surfaces and compared their response with that of distilled water. The results demonstrate that droplet dynamics are governed by the combined interaction of inclination angle, impact inertia, liquid viscosity, and surface roughness, although their relative importance varies with the impact regime. Among all parameters examined, inclination angle was found to be the primary factor controlling spreading asymmetry. As the surface became steeper, gravitational forces increasingly redirected the spreading lamella downslope, producing elongated footprints and enhancing the tendency for instability. The influence of inclination was further amplified by impact inertia, which promoted greater spreading, rim deformation, and splash development. However, the response to increasing inertia depended strongly on liquid properties. Water exhibited extensive downslope spreading and fragmentation, whereas bio-oils maintained comparatively stable and cohesive lamellae because their higher viscosity provided stronger energy dissipation and resistance to rim breakup. The role of surface roughness was found to depend on the balance between inertial forces and contact-line pinning. Under moderate impact conditions, roughness exerted only a limited influence because droplet behaviour was dominated by inclination and fluid properties. As inertia increased, however, roughness became increasingly important by restricting contact-line motion and suppressing lamella instabilities. This transition explains why rough surfaces produced only minor differences in spreading at moderate conditions but effectively prevented splash initiation under more demanding impact regimes. A unified interpretation of the results indicates that stable droplet deposition occurs when viscous dissipation and contact-line pinning are sufficient to counteract the destabilizing effects of gravity and inertia. Bio-oils consistently exhibited greater resistance to splash and fragmentation than water, highlighting the importance of viscosity in maintaining lamella integrity on inclined surfaces. These findings extend the current understanding of droplet impact beyond conventional low-viscosity liquids and provide new insight into the behaviour of renewable fuel droplets on realistic engineering surfaces. From an application perspective, the results suggest that surface inclination and roughness can be used as practical design parameters to control droplet spreading and splash behaviour. Rougher surfaces may be beneficial in applications requiring stable liquid deposition and reduced droplet loss, whereas smoother surfaces may promote greater spreading but increase the risk of splash-induced fragmentation. Such considerations are relevant to biofuel delivery systems, spray cooling technologies, coating processes, and thermal management equipment where liquid retention and deposition uniformity are important. The present study was limited to room-temperature impacts, a specific range of impact conditions, and a selected group of bio-oils. Future work should investigate the influence of surface temperature, wider impact regimes, and additional biofuel formulations to establish generalized scaling relationships capable of predicting droplet behaviour across various fluids and surface conditions.

Acknowledgement
This research was supported by Ministry of Higher Education Malaysia under the Fundamental Research Grant Scheme (FRGS/1/2020/TK0/USM/03/10), and this support is gratefully acknowledged.

References

[1] Jiang, Lei, Qiang Han, Nini Wang, Ming Gao, Suoying He, Hongjun Guan, and Xiaohui Tan. "The effects of water droplet diameter distribution in the rain zone on the cooling capacity and water-splashing noise for natural draft wet cooling towers." *International Journal of Thermal Sciences* 164 (2021): 106875. https://doi.org/10.1016/j.ijthermalsci.2021.106875

[2] Gonome, H., and Wakabayashi, K. (2020). Applications using nano- and microsized droplets and bubbles. *Applied Thermal Engineering*, 171, 115083. https://doi.org/10.1016/j.applthermaleng.2020.115083

[3] Kang, Chao, Motoki Sakaguchi, Ayumi Amano, Yu Kurokawa, and Hirotsugu Inoue. "Quenching stress and fracture of paraffin droplet during solidification and adhesion on metallic substrate." *Surface and Coatings Technology* 374 (2019): 868-877. https://doi.org/10.1016/j.surfcoat.2019.06.067

[4] Del Nevo, A., A. Ciampichetti, M. Tarantino, L. Burgazzi, and Nicola Forgione. "Addressing the heavy liquid metal–Water interaction issue in LBE system." *Progress in Nuclear Energy* 89 (2016): 204-212. https://doi.org/10.1016/j.pnucene.2015.05.006

[5] Liu, Li, Bingbin Ying, Hanyang Gu, Dehui Xu, Chao Huang, and Shuo Chen. "Experimental study on the separation performance of a full-scale SG steam-water separator." *Annals of Nuclear Energy* 141 (2020): 107330. https://doi.org/10.1016/j.anucene.2020.107330

[6] Lipson, N., and S. Chandra. "Cooling of porous metal surfaces by droplet impact." *International Journal of Heat and Mass Transfer* 152 (2020): 119494. https://doi.org/10.1016/j.anucene.2020.107330

[7] Zhao, Peng, Graham K. Hargrave, Hendrik K. Versteeg, Colin P. Garner, Benjamin A. Reid, E. J. Long, and Huayong Zhao. "The dynamics of droplet impact on a heated porous surface." *Chemical Engineering Science* 190 (2018): 232-247. https://doi.org/10.1016/j.ces.2018.06.030

[8] Aliabadi, Mohammad Ali Faghih, Esmail Lakzian, Ali Jahangiri, and Iman Khazaei. "Numerical investigation of effects polydispersed droplets on the erosion rate and condensation loss in the wet steam flow in the turbine blade cascade." *Applied Thermal Engineering* 164 (2020): 114478. https://doi.org/10.1016/j.applthermaleng.2019.114478

[9] Suo, Shaoyi, Ming Jia, Hong Liu, and Tianyou Wang. "Development of a new hybrid stochastic/trajectory droplet collision model for spray simulations in internal combustion engines." *International Journal of Multiphase Flow* 137 (2021): 103581. https://doi.org/10.1016/j.ijmultiphaseflow.2021.103581

[10] Diemuodeke, Ogheneruona E., and Ilai Sher. "Analytical modelling of laminar drag and freestream turbulence eddies on droplet breakup criterion for internal combustion engines." *Proceedings of the Institution of Mechanical Engineers, Part D: Journal of Automobile Engineering* 235, no. 7 (2021): 1956-1965. https://doi.org/10.1177/0954407020980845

[11] Qin, Mengxiao, Yang Guo, Chenglong Tang, Peng Zhang, and Zuohua Huang. "Spreading and bouncing of liquid alkane droplets upon impacting on a heated surface." *International Journal of Heat and Mass Transfer* 159 (2020): 120076. https://doi.org/10.1016/j.ijheatmasstransfer.2020.120076

[12] Hamdan, Khaleel Sami, Dong-Eok Kim, and Sang-Ki Moon. "Droplets behavior impacting on a hot surface above the Leidenfrost temperature." *Annals of Nuclear Energy* 80 (2015): 338-347. https://doi.org/10.1016/j.anucene.2015.02.021

[13] Mehrizi, Abbasali Abouei, Lijie Sun, Jun Zhang, Bo Pang, Kai Zhang, and Longquan Chen. "Droplet impact dynamics on a flexible superhydrophobic cantilever wire mesh." *Surfaces and Interfaces* 44 (2024): 103736. https://doi.org/10.1016/j.surfin.2023.103736

[14] Tian, Wenlong, Huang Zhang, and Qianfeng Liu. "Experimental study on single droplet impinging on a heated and inclined wall at early impaction stage." *Annals of Nuclear Energy* 147 (2020): 107697. https://doi.org/10.1016/j.anucene.2020.107697

[15] Liang, Gangtao, Xingsen Mu, Yali Guo, Shengqiang Shen, Shenglin Quan, and Jili Zhang. "Contact vaporization of an impacting drop on heated surfaces." *Experimental Thermal and Fluid Science* 74 (2016): 73-80. https://doi.org/10.1016/j.expthermflusci.2015.11.027

[16] Cruz, Patrick James, Pierre-Paul De Breuck, Gian-Marco Rignanese, Karine Glinel, and Alain M. Jonas. "Influence of Roughness and Coating on the Rebound of Droplets on Fabrics." *Surfaces and Interfaces* 36 (2023): 102524. https://doi.org/10.1016/j.surfin.2022.102524

[17] Castanet, Guillaume, Ophélie Caballina, W. Chaze, R. Collignon, and F. Lemoine. "The Leidenfrost transition of water droplets impinging onto a superheated surface." *International Journal of Heat and Mass Transfer* 160 (2020): 120126. https://doi.org/10.1016/j.ijheatmasstransfer.2020.120126

[18] Dirbude, Sumer, Vinayak Eswaran, and Abhijit Kushari. "Droplet vaporization modeling of rapeseed and sunflower methyl esters." *Fuel* 92, no. 1 (2012): 171-179. https://doi.org/10.1016/j.fuel.2011.07.030

[19] Sen, S., V. Vaikuntanathan, and D. Sivakumar. "Experimental investigation of biofuel drop impact on stainless steel surface." *Experimental thermal and fluid science* 54 (2014): 38-46. https://doi.org/10.1016/j.expthermflusci.2014.01.014

[20] Li, Cong, Jiali Wang, Linlu Zheng, Zhimin Wang, Quanyi Liu, and Rui Yang. "Experiment study on adhesion dynamic characteristics of droplet impacting on an inclined heated surface." *Surfaces and Interfaces* 51 (2024): 104602. https://doi.org/10.1016/j.surfin.2024.104602

[21] Sazhin, S. S., Al Qubeissi, M., Kolodnytska, R., Elwardany, A. E., Nasiri, R., and Heikal, M. R. (2014). Modelling of biodiesel fuel droplet heating and evaporation. *Fuel*, 115, 559–572. https://doi.org/10.1016/j.fuel.2013.07.031

[22] Saha, Kaushik, Ehab Abu-Ramadan, and Xianguo Li. "Multicomponent evaporation model for pure and blended biodiesel droplets in high temperature convective environment." *Applied Energy* 93 (2012): 71-79. https://doi.org/10.1016/j.fuel.2013.07.031

[23] Morin, Celine, Christian Chauveau, and Iskender Gökalp. "Droplet vaporisation characteristics of vegetable oil derived biofuels at high temperatures." *Experimental Thermal and Fluid Science* 21, no. 1-3 (2000): 41-50. https://doi.org/10.1016/S0894-1777(99)00052-7

[24] Ferrão, Inês, Daniel Vasconcelos, Daniela Ribeiro, André Silva, and Jorge Barata. "A study of droplet deformation: The effect of crossflow velocity on jet fuel and biofuel droplets impinging onto a dry smooth surface." *Fuel* 279 (2020): 118321. https://doi.org/10.1016/j.fuel.2020.118321

[25] Šikalo, Š., Cameron Tropea, and E. N. Ganić. "Impact of droplets onto inclined surfaces." *Journal of colloid and interface science* 286, no. 2 (2005): 661-669. https://doi.org/10.1016/j.jcis.2005.01.050

[26] Josserand, Christophe, and Sigurdur T. Thoroddsen. "Drop impact on a solid surface." *Annual review of fluid mechanics* 48, no. 1 (2016): 365-391. https://doi.org/10.1146/annurev-fluid-122414-034401

[27] Wang, Hao, Cong Liu, Haiyang Zhan, and Yahua Liu. "Droplet asymmetric bouncing on inclined superhydrophobic surfaces." *ACS omega* 4, no. 7 (2019): 12238-12243. https://doi.org/10.1021/acsomega.9b01348

[28] Che, Zhizhao, Amandine Deygas, and Omar K. Matar. "Impact of droplets on inclined flowing liquid films." *Physical Review E* 92, no. 2 (2015): 023032. https://doi.org/10.1103/PhysRevE.92.023032

[29] Tang, Chenglong, Mengxiao Qin, Xinyan Weng, Xuhui Zhang, Peng Zhang, Jianling Li, and Zuohua Huang. "Dynamics of droplet impact on solid surface with different roughness." *International Journal of Multiphase Flow* 96 (2017): 56-69. https://doi.org/10.1016/j.ijmultiphaseflow.2017.07.002

[30] Wang, Lingzi, Jianmei Feng, Tiendat Dang, and Xueyuan Peng. "Dynamics of oil droplet impacting and wetting on the inclined surfaces with different roughness." *International Journal of Multiphase Flow* 135 (2021): 103501. https://doi.org/10.1016/j.ijmultiphaseflow.2020.103501

[31] Moon, Joo Hyun, Minhaeng Cho, and Seong Hyuk Lee. "Dynamic wetting and heat transfer characteristics of a liquid droplet impinging on heated textured surfaces." *International Journal of Heat and Mass Transfer* 97 (2016): 308-317. https://doi.org/10.1016/j.ijheatmasstransfer.2016.02.041